

# A polynomial dimensional decomposition framework based on topology derivatives for stochastic topology sensitivity analysis of high-dimensional complex systems and a type of benchmark problems

Xuchun Ren

<sup>a</sup>*Mechanical Engineering Department, Georgia Southern University, Statesboro, GA, USA*

---

## Abstract

In this paper, a new computational framework based on the topology derivative concept is presented for evaluating stochastic topological sensitivities of complex systems. The proposed framework, designed for dealing with high dimensional random inputs, dovetails a polynomial dimensional decomposition (PDD) of multivariate stochastic response functions and deterministic topology derivatives. On one hand, it provides analytical expressions to calculate topology sensitivities of the first three stochastic moments which are often required in robust topology optimization (RTO). On another hand, it offers embedded Monte Carlo Simulation (MCS) and finite difference formulations to estimate topology sensitivities of failure probability for reliability-based topology optimization (RBTO). For both cases, the quantification of uncertainties and their topology sensitivities are determined concurrently from a single stochastic analysis. Moreover, an original example of two random variables is developed for the first time to obtain analytical solutions for topology sensitivity of moments and failure probability. Another 53-dimension example is constructed for analytical solutions of topology sensitivity of moments and semi-analytical solutions of topology sensitivity of failure probabilities in order to verify the accuracy and efficiency of the proposed method for high-dimensional scenarios. Those examples are new and make it possible for researchers to benchmark stochastic topology sensitivities of existing or new algorithms. In addition, it is unveiled that under certain conditions the proposed method achieves better accuracies for stochastic topology sensitivities than for the stochastic quantities themselves.

*Keywords:* stochastic topology sensitivity analysis, topology derivatives, polynomial dimensional decomposition, stochastic moments, reliability

---

## 1. Introduction

With the rise of additive manufacturing, topology optimization becomes a popular design methodology to determine the optimal distribution of materials in complex engineering structures[1, 2, 3, 4]. Inevitable uncertainties in the additive manufacturing process and operating environment often undermine the performance of such topology designs. Classical deterministic design approaches often lead to unknowingly risky designs due to the underestimation of uncertainties, or inefficient and conservative designs that overcompensate for uncertainties. In the past decade, robust topology optimization (RTO) and reliability-based topology optimization (RBTO) are increasingly adopted as an enabling technology for topology design subject to uncertainty in aerospace, automotive, civil engineering, and additive manufacturing [5, 6, 7, 8, 9, 10, 11]. The former seeks for insensitive topology design via minimizing the propagation of input uncertainty, whereas the latter delivers reliable topology design by introducing probabilistic characterizations of response functions into the objective and/or constraints.

RTO and RBTO for realistic engineering applications confront two challenges: (1) the theoretically infinite-dimensional design vector; and (2) high-dimensional integration resulted from a large number of random variables. Both lead to the curse of dimensionality, which hinders or invalidates almost all RTO and RBTO methods. In RTO, the objective or

---

\*Corresponding author

Email address: NHABEL@gmail.com; xuchun.ren777@gmail.com (Xuchun Ren)

constraint functions are usually expressed by first two moment properties, such as means and standard deviations, of certain stochastic responses, describing the objective robustness or feasibility robustness of a given topology. RBTO often contains probabilistic constraint functions, which restrict the probability of failure regarding certain failure mechanisms. Therefore, to solve a practical RTO or RBTO problem using gradient-based algorithm, an efficient and accurate method for statistical moments, reliability, and their sensitivity analysis of random responses are in demands. The fundamental problem rooted in statistical moment or reliability analyses entails the evaluation of a high-dimensional integral in the entire support of random inputs or its unknown subdomain, respectively. In general, such an integral cannot be calculated analytically. Direct numerical quadrature can be applied, but it is computationally prohibitive when the number of random inputs exceeds three or four, especially when the evaluation of a response function is carried out by expensive finite element analyses (FEA). Existing approaches for statistical moment and reliability analysis include the point estimate method (PEM) [12], Taylor series expansion or perturbation method [12], tensor product quadrature (TPQ) [13], Neumann expansion method [14], the first-order reliability method or FORM-based methods [15, 16, 17, 18, 19, 20], polynomial chaos expansion (PCE) [21], statistically equivalent solution [22], dimension-reduction method [23, 24], and others [25]. Their topology sensitivities have relied mainly on two kinds of approaches: SIMP-based approaches (solid isotropic material with penalization) [26] and topology-derivative-based approaches [27, 28]. The former is based on a fictitious density field representing a smooth transition between material and empty, which requires regularization procedures to get a clear topology. The latter introduces the topological derivative concept which defines the derivative of functionals whose variable is a geometrical domain with respect to singular topology perturbation. The topological derivative concept is mathematically rigorous and independent of the fictitious density field.

Nonetheless, three major concerns arise when evaluating stochastic quantities and their sensitivity using existing approaches or techniques. First, when applied to large-scale topology optimization subject to a large number of random inputs, many of those methods including Taylor series expansions, FORM-based methods, PEM, PCE, TPQ, and dimension-reduction methods, etc. begin to be inapplicable or inadequate. For example, although the Taylor series expansion, FORM-based methods, and PEM are inexpensive and simple, they deteriorate due to the lack of accuracy when the nonlinearity of a response function is high and/or when the input uncertainty is large. PCE approximates the random response via an infinite series of Hermite polynomials of Gaussian variables (or others) and is popular in stochastic mechanics in the last decades. Although truncated forms of PCE were extensively used in practice [29, 30], it is easily succumbed to the curse of dimensionality due to astronomically large numbers of terms or coefficients required to capture the interaction effects between random inputs when applied to high-dimensional systems. Rooted in the referential dimensional decomposition (RDD), the dimension-reduction approximates a high dimensional function via a set of low dimensional components, but it often results in sub-optimal estimations of the original function, and thus its stochastic moments and the associated reliability. Second, to evaluate the topology sensitivity of stochastic quantities, many of the aforementioned methods may not be adequately efficient and accurate. Most of those methods rely on a fictitious density field, thus the sensitivities supplied are not the exact topology sensitivity. Furthermore, many of them resort to repetitive stochastic analyses especially for the sensitivity of reliability due to employed finite-difference techniques, which restrain their computational efficiency. Although Taylor series expansions, is able to perform stochastic sensitivities analysis economically, its accuracy is usually deteriorated by inherited errors from the associated stochastic analysis. Third, to the best of the author's knowledge, in existing literature, there is no benchmark example that provides analytical or semi-analytical solutions for stochastic topology sensitivity analysis. A successful benchmark example certainly calls for analytical expressions of stress, strain, or other response functions in two domains - an original domain and a perforated domain - subject to the same loads and supports. These analytical expressions generally are not readily available even for simple domain and ordinary load cases. Moreover, verifying the performance of a certain method subject to high-dimensional random inputs often demands the benchmark example carrying on complex loads to accommodate a large number of random variables, which impede the implementation of analytical solution of stochastic topology sensitivity. These difficulties result in the lack of benchmark examples and make it impossible to verify the accuracy of existing and new algorithms, especially for high-dimensional cases.

This paper presents a novel framework for topology sensitivity analysis of statistical moments and reliability for complex engineering structures subject to a large number of random inputs. The framework, designed for dealing high-dimensional random inputs, is grounded on the polynomial dimensional decomposition (PDD), and thus it is capable of approximating the high-dimensional stochastic responses in an efficient and accurate manner. It also dovetails

the deterministic topology derivatives with PDD and provides stochastic sensitivities in the exactly topological sense. For RTO, the proposed framework is endowed with analytical expressions for topology sensitivities of the first three stochastic moments. For RBTO, it supplies embedded Monte Carlo Simulation (MCS) and a finite difference formulation to estimate topology sensitivities of failure probability. Furthermore, the evaluation of moments and/or reliability and their topology sensitivity is accomplished concurrently from only a single stochastic analysis. It is noteworthy that two benchmark examples, which provide analytical/semi-analytical topology sensitivity of moments and reliability, are developed for the calibration of stochastic topology sensitivity algorithms. The first example contains only two random variables but provides analytical expressions for moments, reliability, and their topology sensitivities. The second one accommodates 53 random variables, whereas the analytical expressions provided can be easily expanded to any positive number of random variables. The rest of this paper is organized as follows. Section 2 formally defines general RTO and RBTO problems, including a concomitant mathematical statement. Section 3 starts with a brief exposition of the polynomial dimensional decomposition and associated approximations, which result in explicit formulae for the first two moments and an embedded MCS formulation for the reliability of a generic stochastic response. Section 4 revisits the definition of topology derivative and describes the new framework of stochastic topology sensitivity analysis, which integrates PDD and deterministic topological derivative as well as numerical procedures for topology sensitivities of both stochastic moment and reliability. The calculation of PDD expansion coefficients is briefly described in Section 5. Section 6 presents three numerical examples. Two benchmark examples are developed to probe the accuracy and computational efforts of the proposed method. One three-dimensional bracket is used to demonstrate the feasibility of the new method for practical engineering applications. Finally, conclusions are drawn in Section 7.

## 2. Stochastic topology design problems

In the presence of uncertainties, a topology optimization problem can include robust, probabilistic, or non-probabilistic constraints. For RTO, both objective and constraint functions may involve the first two moment properties for the assessment of robustness [31]. Whereas for RBTO, probabilistic functions are often embedded as constraints to restrict the failure probability and achieve a high confidence level on design [32, 16]. Nonetheless, the typical RTO and RBTO problems interested in this paper are often formulated as the following mathematical programming problems

$$\begin{aligned} \min_{\Omega \in D} \quad & c_0(\Omega) := w_1 \frac{\mathbb{E}[y_0(\Omega, \mathbf{X})]}{\mu_0^*} + w_2 \frac{\sqrt{\text{var}[y_0(\Omega, \mathbf{X})]}}{\sigma_0^*}, \\ \text{subject to} \quad & c_k(\Omega) := \alpha_k \sqrt{\text{var}[y_k(\Omega, \mathbf{X})]} - \mathbb{E}[y_k(\Omega, \mathbf{X})] \leq 0; \quad k = 1, \dots, K \end{aligned} \quad (1)$$

and

$$\begin{aligned} \min_{\Omega \in D} \quad & c_0(\Omega) := w_1 \frac{\mathbb{E}[y_0(\Omega, \mathbf{X})]}{\mu_0^*} + w_2 \frac{\sqrt{\text{var}[y_0(\Omega, \mathbf{X})]}}{\sigma_0^*}, \\ \text{subject to} \quad & c_k(\Omega) := P[\mathbf{X} \in \Omega_{F,k}] \leq p_k; \quad k = 1, \dots, K, \end{aligned} \quad (2)$$

respectively, where  $D \subset \mathbb{R}^3$  is a bounded domain in which all admissible topology design  $\Omega$  are included;  $\mathbf{X} := (X_1, \dots, X_N)^T \in \mathbb{R}^N$  is an  $N$ -dimensional random input vector completely defined by a family of joint probability density functions  $\{f_{\mathbf{X}}(\mathbf{x}), \mathbf{x} \in \mathbb{R}^N\}$  on the probability triple  $(\Omega_{\mathbf{X}}, \mathcal{F}, P)$ , where  $\Omega_{\mathbf{X}}$  is the sample space;  $\mathcal{F}$  is the  $\sigma$ -field on  $\Omega_{\mathbf{X}}$ ;  $P$  is the probability measure associated with probability density  $f_{\mathbf{X}}(\mathbf{x})$ ;  $\Omega_{F,k}$  is the  $k$ th failure domain defined by response function  $y_k(\Omega, \mathbf{X})$ ;  $0 < p_k < 1$  expresses target failure probabilities;  $w_1 \in \mathbb{R}_0^+$  and  $w_2 \in \mathbb{R}_0^+$  are two non-negative, real-valued weights, satisfying  $w_1 + w_2 = 1$ ,  $\mu_0^* \in \mathbb{R} \setminus \{0\}$  and  $\sigma_0^* \in \mathbb{R}^+$  are two non-zero, real-valued scaling factors;  $\alpha_k \in \mathbb{R}^+$ ,  $k = 0, 1, \dots, K$ , are positive, real-valued constants associated with the probabilities of constraint satisfaction;  $\mathbb{E}$  and  $\text{var}$  are expectation operator and variance operator, respectively, with respect to

the probability measure  $P$ . The evaluation of both  $\mathbb{E}$  and var on certain random response demands statistical moment analysis [33, 34, 35, 36, 37, 14, 22, 23, 24, 25], which is not unduly difficult. By contrast, the evaluation of probabilistic constraint functions in RBTO, generally more complicated than  $\mathbb{E}$  and var, is obtained from

$$c_k(\Omega) := P[\mathbf{X} \in \Omega_{F,k}] = \int_{\Omega_{F,k}} f_{\mathbf{X}}(\mathbf{x}) d\mathbf{x} = \int_{\mathbb{R}^N} I_{\Omega_{F,k}}(\Omega, \mathbf{x}) d\mathbf{x} := \mathbb{E}[I_{\Omega_{F,k}}(\Omega, \mathbf{X})] \quad (3)$$

which represents a failure probability from *reliability analysis* [38, 39, 40, 41, 42, 43, 44, 45, 46, 47]. The indicator function  $I_{\Omega_{F,k}}(\Omega, \mathbf{x}) = 1$  when  $\mathbf{x} \in \Omega_{F,k}$  and *zero* otherwise. For component-level RBTO, the failure domain, often adequately described by a single performance function  $y_k(\Omega, \mathbf{x})$ , and component reliability analysis are relatively simple. Whereas, interdependent performance functions  $y_k^{(q)}(\Omega, \mathbf{x})$ ,  $q = 1, 2, \dots$ , are required for a system-level (series, parallel, or general) RBTO, leading to a highly complex failure domain and huge computational demand for system reliability analysis.

### 3. Polynomial dimensional decomposition method and uncertainty quantification

#### 3.1. Polynomial dimensional decomposition

Consider a multivariate stochastic response  $y(\Omega, \mathbf{X})$  of certain topology design  $\Omega$  subject to random input vector  $\mathbf{X} = \{X_1, \dots, X_N\}^T$ , representing any of the performance function  $y_k$  in Eq. (1) or (2). Let  $\mathcal{L}_2(\Omega_{\mathbf{X}}, \mathcal{F}, P)$  be a Hilbert space of square-integrable functions  $y$  with a probability measure  $f_{\mathbf{X}}(\mathbf{x}) d\mathbf{x}$  supported on  $\mathbb{R}^N$ . Assuming independent components of  $\mathbf{X}$ , the PDD expansion of function  $y$  generates a hierarchical representation [48, 49]

$$y(\Omega, \mathbf{X}) = y_0(\Omega) + \sum_{\emptyset \neq u \subseteq \{1, \dots, N\}} \sum_{\mathbf{j}_{|u|} \in \mathbb{N}^{|u|}} C_{u\mathbf{j}_{|u|}}(\Omega) \psi_{u\mathbf{j}_{|u|}}(\mathbf{X}_u; \Omega), \quad (4)$$

of the original performance function, in terms of an infinite number of multivariate orthonormal basis [48, 49]  $\psi_{u\mathbf{j}_{|u|}}(\mathbf{X}_u; \Omega) := \prod_{p=1}^{|u|} \psi_{i_p, j_p}(X_{i_p}; \Omega)$  in  $\mathcal{L}_2(\Omega_{\mathbf{X}}, \mathcal{F}, P)$ , where  $\mathbf{j}_{|u|} = (j_1, \dots, j_{|u|}) \in \mathbb{N}^{|u|}$  is a  $|u|$ -dimensional multi-index;  $y_0(\Omega)$  contributes the constant component; for  $|u| = 1$ ,  $C_{u\mathbf{j}_{|u|}}(\Omega) \psi_{u\mathbf{j}_{|u|}}(\mathbf{X}_u; \Omega)$  commits all univariate component functions representing the individual contribution to  $y(\Omega, \mathbf{X})$  from each single input variable; for  $|u| = 2$ , it brings in all bivariate component functions embodying the cooperative influence of any two input variables; and for  $|u| = S$ , it admits  $S$ -variate component functions quantifying the interactive effects of any  $S$  input variables. For most performance functions in engineering applications, a truncated version of Eq. (4) is often accurate enough by retaining, at most, the interactive effects of  $S < N$  input variables and  $m$ th order polynomials,

$$\tilde{y}_{S,m}(\Omega, \mathbf{X}) = y_0(\Omega) + \sum_{\substack{\emptyset \neq u \subseteq \{1, \dots, N\} \\ 1 \leq |u| \leq S}} \sum_{\substack{\mathbf{j}_{|u|} \in \mathbb{N}^{|u|} \\ \|\mathbf{j}_{|u|}\|_{\infty} \leq m}} C_{u\mathbf{j}_{|u|}}(\Omega) \psi_{u\mathbf{j}_{|u|}}(\mathbf{X}_u; \Omega), \quad (5)$$

where

$$y_0(\Omega) = \int_{\mathbb{R}^N} y(\mathbf{x}, \Omega) f_{\mathbf{X}}(\mathbf{x}) d\mathbf{x} \quad (6)$$

and

$$C_{u\mathbf{j}_{|u|}}(\Omega) := \int_{\mathbb{R}^N} y(\mathbf{x}, \Omega) \psi_{u\mathbf{j}_{|u|}}(\mathbf{x}_u; \Omega) f_{\mathbf{X}}(\mathbf{x}) d\mathbf{x}, \quad \emptyset \neq u \subseteq \{1, \dots, N\}, \mathbf{j}_{|u|} \in \mathbb{N}^{|u|}, \quad (7)$$

are referred to as expansion coefficients of PDD expansion (4) or truncated PDD approximation (5). The untruncated PDD expansion in Eq. (4) employs an orthogonal polynomial basis and exactly represents the response function, it can be easily refer that it is equivalent to PCE when the basis used is same. However, the PDD expansion provides a hierarchical representation by classifying the interaction between random inputs, which is a key to alleviate the course of dimensionality when applying its truncated version. For  $S > 0$  and  $m > 0$ , Eq. (5) retains interactive effects among at most  $S$  input variables  $X_{i_1}, \dots, X_{i_S}$ ,  $1 \leq i_1 < \dots < i_S \leq N$  and  $m$ th order polynomial nonlinearity in  $y$ , thus leading to the so-called  $S$ -variate,  $m$ th-order PDD approximation. When  $S \rightarrow N$  and  $m \rightarrow \infty$ ,  $\tilde{y}_{S,m}$  converges to  $y$  in the mean-square sense and engenders a sequence of hierarchical and convergent approximations of  $y$ . Based on the dimensional

structure and nonlinearity of a stochastic response, the truncation parameters  $S$  and  $m$  can be chosen correspondingly. The higher the values of  $S$  and  $m$  permit the higher the accuracy, but also endow the computational cost of an  $S$ th-order polynomial computational complexity [48, 49]. Henceforth, the  $S$ -variate,  $m$ th-order PDD approximation will be simply referred to as *truncated PDD approximation* in this paper.

### 3.2. Stochastic moment analysis

For an arbitrary random response of certain topology design  $\Omega$ , let  $m^{(r)}(\Omega) := \mathbb{E}[y^r(\Omega, \mathbf{X})]$ , if it exists, denote the raw moment of  $y$  of order  $r$ , where  $r \in \mathbb{N}$ . Let  $\tilde{m}^{(r)}(\Omega) := \mathbb{E}[\tilde{y}_{S,m}^r(\Omega, \mathbf{X})]$  denote the raw moment of  $\tilde{y}_{S,m}$  of order  $r$ , given an  $S$ -variate,  $m$ th-order PDD approximation  $\tilde{y}_{S,m}(\Omega, \mathbf{X})$  of  $y(\Omega, \mathbf{X})$ . The analytical expressions or explicit formulae for estimating the moments using PDD approximations are described as follows. Applying the expectation operator on  $\tilde{y}_{S,m}(\Omega, \mathbf{X})$  and  $\tilde{y}_{S,m}^2(\Omega, \mathbf{X})$ , the first moment or mean [50]

$$\tilde{m}_{S,m}^{(1)}(\Omega) := \mathbb{E}[\tilde{y}_{S,m}(\Omega, \mathbf{X})] = y_0(\Omega) = \mathbb{E}[y(\Omega, \mathbf{X})] =: m^{(1)}(\Omega) \quad (8)$$

of the  $S$ -variate,  $m$ th-order PDD approximation is simply the constant component in Eq. (5), whereas the second moment [50]

$$\tilde{m}_{S,m}^{(2)}(\Omega) := \mathbb{E}[\tilde{y}_{S,m}^2(\Omega, \mathbf{X})] = y_0^2(\Omega) + \sum_{\substack{0 \neq u \subseteq \{1, \dots, N\} \\ 1 \leq |u| \leq S}} \sum_{\substack{\mathbf{j}_{|u|} \in \mathbb{N}^{|u|} \\ \|\mathbf{j}_{|u|}\|_{\infty} \leq m}} C_{u\mathbf{j}_{|u|}}^2(\Omega) \quad (9)$$

is expressed as the sum of squares of all expansion coefficients of  $\tilde{y}_{S,m}(\Omega, \mathbf{X})$ . It is straightforward that the estimation of the second moment evaluated by Eq. (9) approaches the exact second moment

$$m^{(2)}(\Omega) := \mathbb{E}[y^2(\Omega, \mathbf{X})] = y_0^2(\Omega) + \sum_{0 \neq u \subseteq \{1, \dots, N\}} \sum_{\mathbf{j}_{|u|} \in \mathbb{N}^{|u|}} C_{u\mathbf{j}_{|u|}}^2(\Omega) \quad (10)$$

of  $y$  when  $S \rightarrow N$  and  $m \rightarrow \infty$ . The mean-square convergence of  $\tilde{y}_{S,m}$  is ensured as its component functions will contain all required bases of the corresponding Hilbert spaces. Furthermore, the variance of  $\tilde{y}_{S,m}(\Omega, \mathbf{X})$  is also mean-square convergent.

### 3.3. Reliability analysis

The RBTO problem defined in Eq. (2) requires not only stochastic moment analysis but also evaluations of the probabilistic constraints, that is, the failure probability

$$P_F = P[\mathbf{X} \in \Omega_{F,k}] = \int_{\Omega_{F,k}} f_{\mathbf{X}}(\mathbf{x}) d\mathbf{x} = \int_{\mathbb{R}^N} I_{\Omega_{F,k}}(\Omega, \mathbf{x}) d\mathbf{x} := \mathbb{E}[I_{\Omega_{F,k}}(\Omega, \mathbf{X})] \quad (11)$$

of a certain topology design  $\Omega$  with respect to certain failure set  $\Omega_{F,k}$ . In which, the indicator function  $I_{\Omega_{F,k}}(\Omega, \mathbf{x}) = 1$  when  $\mathbf{x} \in \Omega_{F,k}$  and *zero* otherwise. For component-level RBTO, the failure set is often adequately characterized by a single performance function  $y_k(\Omega, \mathbf{x})$  as  $\Omega_{F,k} := \{\mathbf{x} : y_k(\Omega, \mathbf{x}) < 0\}$ . Whereas for a system-level RBTO, it is usually described by multiple, interdependent performance functions  $y_k^{(q)}(\Omega, \mathbf{x})$ ,  $q = 1, 2, \dots$ , leading, for example, to  $\Omega_{F,k} := \{\mathbf{x} : \cup_q y_k^{(q)}(\Omega, \mathbf{x}) < 0\}$  and  $\Omega_{F,k} := \{\mathbf{x} : \cap_q y_k^{(q)}(\Omega, \mathbf{x}) < 0\}$  for series and parallel systems, respectively. Let  $\tilde{\Omega}_{F,k} := \{\mathbf{x} : \tilde{y}_{S,m}(\mathbf{x}) < 0\}$  or  $\tilde{\Omega}_{F,k} := \{\mathbf{x} : \cup_q \tilde{y}_{S,m}^{(q)}(\mathbf{x}) < 0\}$  or  $\tilde{\Omega}_{F,k} := \{\mathbf{x} : \cap_q \tilde{y}_{S,m}^{(q)}(\mathbf{x}) < 0\}$  be an approximate failure set as a result of  $S$ -variate,  $m$ th-order PDD approximations  $\tilde{y}_{S,m}(\mathbf{X})$  of  $y(\mathbf{X})$  or  $\tilde{y}_{S,m}^{(q)}(\mathbf{X})$  of  $y^{(q)}(\mathbf{X})$ . Then the embedded MCS estimate of the failure probability  $P_F$  is

$$\tilde{P}_F = \mathbb{E}_{\mathbf{d}}[I_{\tilde{\Omega}_{F,k}}(\Omega, \mathbf{X})] = \lim_{L \rightarrow \infty} \frac{1}{L} \sum_{l=1}^L I_{\tilde{\Omega}_{F,k}}(\Omega, \mathbf{x}^{(l)}), \quad (12)$$

where  $L$  is the sample size,  $\mathbf{x}^{(l)}$  is the  $l$ th realization of  $\mathbf{X}$ , and  $I_{\tilde{\Omega}_{F,k}}(\Omega, \mathbf{x})$ , equal to *one* when  $\mathbf{x} \in \tilde{\Omega}_{F,k}$  and *zero* otherwise, is an approximation of the indicator function  $I_{\Omega_{F,k}}(\Omega, \mathbf{x})$ .

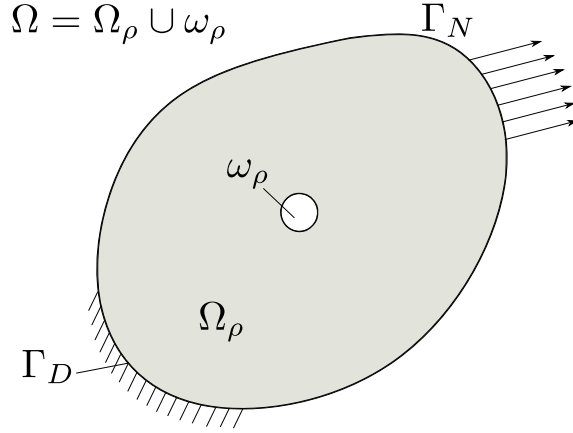


Figure 1: A perforated domain

Note that the stochastic moment analysis and reliability analysis for RTO and RBTO are quite similar to the ones in a general robust design optimization (RDO) and reliability-based design optimization (RBDO) [51, 52, 53] except that the former is affiliated with certain topology designs  $\Omega$ . However, topology sensitivity analysis of moments and reliability is distinct from sensitivity analysis in RDO and RBDO due to the disparate topology change associated, and is elaborated in the next section.

#### 4. Stochastic topology sensitivity analysis

To evaluate the topology sensitivity of a stochastic response, a new framework is proposed here which dovetails PDD and deterministic topological derivative. It relies fundamentally on the topology derivative [54, 55, 56, 57, 58, 59, 60, 61, 62] of a deterministic objective function  $y(\Omega)$ . The new method provides closed-form solutions and an embedded MCS formulation for the topological derivative of stochastic moments and reliability, respectively. Before presenting the new framework itself, a brief revisit on the idea of topological derivative appears to be necessary and should be convenient to those not yet familiar with the concept.

##### 4.1. Topological derivative - revisit

Pioneered by Schumacher[63], Sokolowski and Zochowski [64, 65], and Garreau et al. [66], the *topological derivative* measures the change of a performance functional when an infinitesimal hole is introduced in the reference domain in which a boundary-value problem is defined. For a given reference domain  $\Omega \subset \mathbb{R}^n$ , a point  $\xi_0 \in \Omega$ , and a hole  $\omega \in \mathbb{R}^n$  with the radius of 1, a translated and rescaled hole can be defined by  $\omega_\rho = \xi_0 + \rho\omega$ ,  $\forall \rho > 0$  and the perforated domain is  $\Omega_\rho = \Omega \setminus \omega_\rho$  as shown in Fig. 1.

For a small  $\rho > 0$ , if  $y(\Omega_\rho)$  admits the topological asymptotic expansion

$$y(\Omega_\rho) = y(\Omega) + \rho^n D_T y(\xi_0) + o(\rho^n), \quad (13)$$

then  $D_T y(\xi_0)$  is called the topological derivative at point  $\xi_0$  and is applicable to general boundary value problems including the linear elastic system

$$\begin{cases} \nabla \cdot (\mathbb{C} : \nabla \mathbf{u}) = \mathbf{0} & \text{in } \Omega \\ \mathbf{u} = \bar{\mathbf{u}} & \text{on } \Gamma_D \\ \mathbf{n} \cdot (\mathbb{C} : \nabla \mathbf{u}) =: \mathbf{t} = \bar{\mathbf{t}} & \text{on } \Gamma_N \end{cases} \quad (14)$$

where  $\mathbb{C}$  is the elastic tensor,  $\Gamma_D$  and  $\Gamma_N$  denote Dirichlet boundary and Neumann boundary of  $\Omega$ , respectively. The topological asymptotic expansion (13) contains two performance functions  $y(\Omega)$  and  $y(\Omega_\rho)$ . The former is related to



the reference domain  $\Omega$  and evaluated by solving (14), whereas the latter is affiliated with the perforated domain  $\Omega_\rho$  and the associated boundary value problem

$$\begin{cases} \nabla \cdot [\mathbb{C} : \nabla (\mathbf{u} + \hat{\mathbf{u}})] = \mathbf{0} & \text{in } \Omega_\rho \\ \mathbf{u} + \hat{\mathbf{u}} = \bar{\mathbf{u}} & \text{on } \Gamma_D \\ \mathbf{n} \cdot [\mathbb{C} : \nabla (\mathbf{u} + \hat{\mathbf{u}})] =: \mathbf{t} + \hat{\mathbf{t}} = \bar{\mathbf{t}} & \text{on } \Gamma_N \\ \mathbf{t} + \hat{\mathbf{t}} = \mathbf{0} & \text{on } -\partial\omega_\rho \end{cases} \quad (15)$$

where the Neumann type condition is prescribed on  $-\partial\omega_\rho$ , i.e., the boundary  $\partial\omega_\rho$  with the opposite normal vector. Comparing Eq. (14) and Eq. (15), it concludes that  $\hat{\mathbf{u}} = \mathbf{0}$  on  $\Gamma_D$  and  $\hat{\mathbf{t}} = \mathbf{0}$  on  $\Gamma_N$ . Moreover, it was proved that  $\hat{\mathbf{u}} + o(\rho)$ , where  $o(\rho)$  is the reminder of higher order compared to  $\rho$ , is the solution of the following *external problem* [66]

$$\begin{cases} \nabla \cdot (\mathbb{C} : \nabla \hat{\mathbf{u}}) = \mathbf{0} & \text{in } \mathbb{R}^n \setminus \overline{\omega_\rho} \\ \mathbf{n} \cdot (\mathbb{C} : \nabla \hat{\mathbf{u}}) =: \hat{\mathbf{t}} = \mathbf{n} \cdot \mathbb{C} : \nabla \mathbf{u}(\xi_0) & \text{on } -\partial\omega_\rho \end{cases}, \quad (16)$$

as  $\rho \rightarrow 0$ . Solutions  $\hat{\mathbf{u}}$  for various cases of isotropic elasticity are summarized in Table 1, for more details and an easy solution utilizing the *Eshelby tensor*, refer to Appendix A.

Both  $y(\Omega)$  and  $y(\Omega_\rho)$  admit a general class of performance functions. Consider the compliance of the structure as the performance functional,  $y(\Omega) := \int_{\Gamma_D \cup \Gamma_N} \mathbf{u} \cdot \mathbf{t} d\Gamma$ , which can be augmented by a Lagrange multiplier  $\lambda$  to introduce the governing equation as follows,

$$y(\Omega) := \int_{\Gamma_D \cup \Gamma_N} \mathbf{u} \cdot \mathbf{t} d\Gamma = \int_{\Gamma_D \cup \Gamma_N} \mathbf{u} \cdot \mathbf{t} d\Gamma + \int_{\Omega} \lambda \cdot [\nabla \cdot (\mathbb{C} : \nabla \mathbf{u})] d\Omega, \quad (17)$$

by noticing  $\mathbf{u}$  being the solution of Eq. (14) in advance, where  $\lambda$  can be any kinematically admissible field that meets appropriate smoothness requirements. Similarly for the perforated domain,

$$y(\Omega_\rho) := \int_{\Gamma_D \cup \Gamma_N} (\mathbf{u} + \hat{\mathbf{u}}) \cdot (\mathbf{t} + \hat{\mathbf{t}}) d\Gamma + \int_{\Omega_\rho} \lambda \cdot [\nabla \cdot (\mathbb{C} : \nabla (\mathbf{u} + \hat{\mathbf{u}}))] d\Omega. \quad (18)$$

The change of compliance after perforation

$$\begin{aligned} y(\Omega_\rho) - y(\Omega) &= \int_{\Gamma_D \cup \Gamma_N} (\mathbf{u} \cdot \hat{\mathbf{t}} + \hat{\mathbf{u}} \cdot \mathbf{t} + \hat{\mathbf{u}} \cdot \hat{\mathbf{t}}) d\Gamma + \int_{\Omega_\rho} \lambda \cdot [\nabla \cdot (\mathbb{C} : \nabla \hat{\mathbf{u}})] d\Omega - \int_{\omega_\rho} \lambda \cdot [\nabla \cdot (\mathbb{C} : \nabla \mathbf{u})] d\Omega \\ &= \int_{\Gamma_D \cup \Gamma_N} (\mathbf{u} \cdot \hat{\mathbf{t}} + \hat{\mathbf{u}} \cdot \mathbf{t}) d\Gamma + \int_{\Omega_\rho} \lambda \cdot [\nabla \cdot (\mathbb{C} : \nabla \hat{\mathbf{u}})] d\Omega - \int_{\omega_\rho} \lambda \cdot [\nabla \cdot (\mathbb{C} : \nabla \mathbf{u})] d\Omega, \end{aligned} \quad (19)$$

employing  $\hat{\mathbf{u}} \rightarrow \mathbf{0}$  on  $\Gamma_D$  and  $\hat{\mathbf{t}} \rightarrow \mathbf{0}$  on  $\Gamma_N$  as  $\rho \rightarrow 0$ . Integrate the second term of the above equation by parts twice

and the third term one time, meanwhile applying divergence theorem,

$$\begin{aligned}
y(\Omega_\rho) - y(\Omega) &= \int_{\Gamma_D \cup \Gamma_N} (\mathbf{u} \cdot \hat{\mathbf{t}} + \hat{\mathbf{u}} \cdot \mathbf{t}) d\Gamma + \int_{\Gamma_D \cup \Gamma_N \cup \partial\omega_\rho} \lambda \cdot \hat{\mathbf{t}} d\Gamma - \int_{\Omega_\rho} \nabla \lambda : \mathbb{C} : \nabla \hat{\mathbf{u}} d\Omega - \int_{\partial\omega_\rho} \lambda \cdot \mathbf{t} d\Gamma + \int_{\omega_\rho} \nabla \lambda : \mathbb{C} : \nabla \mathbf{u} d\Omega \\
&= \int_{\Gamma_D \cup \Gamma_N} (\mathbf{u} \cdot \hat{\mathbf{t}} + \hat{\mathbf{u}} \cdot \mathbf{t} + \lambda \cdot \hat{\mathbf{t}}) d\Gamma - \int_{\partial\omega_\rho} \lambda \cdot \hat{\mathbf{t}} d\Gamma - \int_{\Gamma_D \cup \Gamma_N \cup \partial\omega_\rho} \hat{\mathbf{u}} \cdot (\mathbf{n} \cdot \mathbb{C} : \nabla \lambda) d\Gamma + \int_{\Omega_\rho} \hat{\mathbf{u}} \cdot [\nabla \cdot (\mathbb{C} : \nabla \lambda)] d\Omega \\
&\quad - \int_{\partial\omega_\rho} \lambda \cdot \mathbf{t} d\Gamma + \int_{\omega_\rho} \nabla \lambda : \mathbb{C} : \nabla \mathbf{u} d\Omega \\
&= \int_{\Gamma_D} (\mathbf{u} + \lambda) \cdot \hat{\mathbf{t}} d\Gamma + \int_{\Gamma_N} \hat{\mathbf{u}} \cdot \mathbf{t} d\Gamma - \int_{\partial\omega_\rho} \lambda \cdot (\mathbf{t} + \hat{\mathbf{t}}) d\Gamma - \int_{\Gamma_N} \hat{\mathbf{u}} \cdot (\mathbf{n} \cdot \mathbb{C} : \nabla \lambda) d\Gamma + \int_{\Omega_\rho} \hat{\mathbf{u}} \cdot [\nabla \cdot (\mathbb{C} : \nabla \lambda)] d\Omega \\
&\quad + \int_{\partial\omega_\rho} \hat{\mathbf{u}} \cdot (\mathbf{n} \cdot \mathbb{C} : \nabla \lambda) d\Gamma + \int_{\omega_\rho} \nabla \lambda : \mathbb{C} : \nabla \mathbf{u} d\Omega \\
&= \int_{\Gamma_D} (\mathbf{u} + \lambda) \cdot \hat{\mathbf{t}} d\Gamma + \int_{\Gamma_N} \hat{\mathbf{u}} \cdot (\mathbf{t} - \mathbf{n} \cdot \mathbb{C} : \nabla \lambda) d\Gamma + \int_{\Omega_\rho} \hat{\mathbf{u}} \cdot [\nabla \cdot (\mathbb{C} : \nabla \lambda)] d\Omega + \int_{\partial\omega_\rho} \hat{\mathbf{u}} \cdot (\mathbf{n} \cdot \mathbb{C} : \nabla \lambda) d\Gamma \\
&\quad + \int_{\omega_\rho} \nabla \lambda : \mathbb{C} : \nabla \mathbf{u} d\Omega, \tag{20}
\end{aligned}$$

noticing  $\hat{\mathbf{u}} = \mathbf{0}$  on  $\Gamma_D$ ,  $\hat{\mathbf{t}} = \mathbf{0}$  on  $\Gamma_N$ ,  $\mathbf{t} + \hat{\mathbf{t}} = \mathbf{0}$  on  $\partial\omega_\rho$ , and  $\mathbf{n}$  is always the normal of the current integration surface during the above derivation. Take  $\lambda$  as the displacement solution of the following adjoint problem

$$\begin{cases} \nabla \cdot (\mathbb{C} : \nabla \lambda) = 0 & \text{in } \Omega \\ \lambda = -\bar{\mathbf{u}} & \text{on } \Gamma_D \\ \mathbf{n} \cdot (\mathbb{C} : \nabla \lambda) = \bar{\mathbf{t}} & \text{on } \Gamma_N \end{cases} \tag{21}$$

and apply the solution  $\hat{\mathbf{u}}$  on  $\partial\omega_\rho$  of the external problem for the three-dimensional case in Table 1, we have

$$\begin{aligned}
y(\Omega_\rho) - y(\Omega) &= \int_{\omega_\rho} \nabla \lambda : \mathbb{C} : \nabla \mathbf{u} d\Omega + \int_{\partial\omega_\rho} \hat{\mathbf{u}} \cdot (\mathbf{n} \cdot \mathbb{C} : \nabla \lambda) d\Gamma \\
&= \frac{4\pi\rho^3}{3} (\mathbb{C}^{-1} : \tilde{\boldsymbol{\sigma}}) : \boldsymbol{\sigma} + \rho \int_{\partial\omega_\rho} \left( \frac{a-b}{3} \text{tr}(\boldsymbol{\sigma}) \mathbf{n} + b\mathbf{n} \cdot \boldsymbol{\sigma} \right) \cdot (\mathbf{n} \cdot \tilde{\boldsymbol{\sigma}}) d\Gamma \\
&= \frac{4\pi\rho^3}{3} \tilde{\boldsymbol{\sigma}} : \mathbb{C}^{-1} : \boldsymbol{\sigma} + \rho \left[ b(\tilde{\boldsymbol{\sigma}} \cdot \boldsymbol{\sigma}) : \int_{\partial\omega_\rho} \mathbf{n} \mathbf{n} d\Gamma + \frac{a-b}{3} \text{tr}(\boldsymbol{\sigma}) \tilde{\boldsymbol{\sigma}} : \int_{\partial\omega_\rho} \mathbf{n} \mathbf{n} d\Gamma \right] \\
&= \frac{4\pi\rho^3}{3} \left[ \tilde{\boldsymbol{\sigma}} : \mathbb{C}^{-1} : \boldsymbol{\sigma} + \left[ b\tilde{\boldsymbol{\sigma}} : \mathbb{I} : \boldsymbol{\sigma} + \frac{a-b}{3} \tilde{\boldsymbol{\sigma}} : \boldsymbol{\delta} \boldsymbol{\delta} : \boldsymbol{\sigma} \right] \right], \tag{22}
\end{aligned}$$

identifying  $\int_{\partial\omega_\rho} \mathbf{n} \mathbf{n} = \frac{4\pi\rho^2}{3} \boldsymbol{\delta}$  for the three-dimensional case, where  $\boldsymbol{\delta}$  is the second-order unit tensor,  $\mathbb{I}$  is the fourth-order identity tensor, and  $\tilde{\boldsymbol{\sigma}} = \mathbb{C} : \nabla \lambda$  is the stress solution at  $\xi_0$  of the adjoint problem. Further calculations lead to

$$\begin{aligned}
y(\Omega_\rho) - y(\Omega) &= \frac{4\pi\rho^3}{3} \tilde{\boldsymbol{\sigma}} : \left[ \left( \frac{(1+\nu)}{E} + b \right) \mathbb{I} + \left( \frac{a-b}{3} - \frac{\nu}{E} \right) \boldsymbol{\delta} \boldsymbol{\delta} \right] : \boldsymbol{\sigma} \\
&= 4\pi\rho^3 \frac{1-\nu}{2E(7-5\nu)} \tilde{\boldsymbol{\sigma}} : [10(1+\nu)\mathbb{I} - (5\nu+1)\boldsymbol{\delta} \boldsymbol{\delta}] : \boldsymbol{\sigma} \\
&:= \rho^3 \tilde{\boldsymbol{\sigma}} : \mathbb{A} : \boldsymbol{\sigma} \tag{23}
\end{aligned}$$

noticing  $\mathbb{C}^{-1} = \frac{1+\nu}{E} \mathbb{I} - \frac{\nu}{E} \boldsymbol{\delta} \boldsymbol{\delta}$  for this case. Therefore the corresponding topological derivative  $D_T y(\Omega, \xi_0)$  has a concrete form

$$D_T y(\Omega, \xi_0) = \tilde{\boldsymbol{\sigma}}(\xi_0) : \mathbb{A} : \boldsymbol{\sigma}(\xi_0), \tag{24}$$



Table 1: Displacement solutions on  $\partial\omega_\rho$  of (16) and tensor  $\mathbb{A}$  for various cases

Isotropic	Displacement on $\partial\omega_\rho$ of Eq. (16)	$\mathbb{A}$
Plane stress	$\rho \left[ \frac{\nu-1}{E} \text{tr}(\boldsymbol{\sigma}(\boldsymbol{\xi}_0)) \mathbf{n} + \frac{3-\nu}{E} \mathbf{n} \cdot \boldsymbol{\sigma}(\boldsymbol{\xi}_0) \right]$	$\frac{\pi}{E} [4\mathbb{I} - \boldsymbol{\delta}\boldsymbol{\delta}]$
Plane strain	$\rho \frac{(1+\nu)}{E} [(2\nu-1) \text{tr}(\boldsymbol{\sigma}(\boldsymbol{\xi}_0)) \mathbf{n} + (3-4\nu) \mathbf{n} \cdot \boldsymbol{\sigma}(\boldsymbol{\xi}_0)]$	$\frac{\pi(1-\nu^2)}{E} [4\mathbb{I} - \boldsymbol{\delta}\boldsymbol{\delta}]$
3D	$\rho \left[ \frac{a-b}{3} \text{tr}(\boldsymbol{\sigma}(\boldsymbol{\xi}_0)) \mathbf{n} + b \mathbf{n} \cdot \boldsymbol{\sigma}(\boldsymbol{\xi}_0) \right]^\dagger$	$\frac{2\pi(1-\nu)}{E(7-5\nu)} [10(1+\nu)\mathbb{I} - (5\nu+1)\boldsymbol{\delta}\boldsymbol{\delta}]$

$^\dagger a = \frac{1+\nu}{2E}, b = \frac{2(4-5\nu^2-\nu)}{E(7-5\nu)}, \boldsymbol{\sigma}(\boldsymbol{\xi}_0) = \mathbb{C} : \boldsymbol{\epsilon}(\boldsymbol{\xi}_0)$ , where  $\mathbf{n}$  is the normal of  $\partial\omega_\rho$

where the fourth-order tensor  $\mathbb{A} = \frac{2\pi(1-\nu)}{E(7-5\nu)} [10(1+\nu)\mathbb{I} - (5\nu+1)\boldsymbol{\delta}\boldsymbol{\delta}]$ . The evaluation of  $D_T y(\Omega, \boldsymbol{\xi}_0)$  requires the stress solution at  $\boldsymbol{\xi}_0$  from both the original problem and the adjoint problem. In the case that  $\bar{\mathbf{u}} = 0$ , the latter becomes self-adjoint and only the solution of Eq. (14) is needed. The expressions of  $\mathbb{A}$  for various cases are summarized in Table 1.

#### 4.2. Topology sensitivity of stochastic moments

Let  $y(\Omega, \mathbf{X})$  be a response function of the linear system (14) subject to random input  $\mathbf{X}$ , which can be uncertain loads, geometry, or material properties. For a point  $\boldsymbol{\xi}_0 \in \Omega$ , taking topology derivative of  $r$ th moments of the response function  $y(\Omega, \mathbf{X})$  and applying the Lebesgue dominated convergence theorem, which permits the interchange of the differential and integral operators, yields

$$D_T m^{(r)}(\Omega, \boldsymbol{\xi}_0) := D_T \mathbb{E} [y^r(\Omega, \mathbf{X})]_{|\boldsymbol{\xi}_0} = \int_{\mathbb{R}^N} r y^{r-1}(\Omega, \mathbf{x}) D_T y(\Omega, \mathbf{x}, \boldsymbol{\xi}_0) f_{\mathbf{X}}(\mathbf{x}) d\mathbf{x} = \mathbb{E} [r y^{r-1}(\Omega, \mathbf{X}) D_T y(\Omega, \mathbf{X}, \boldsymbol{\xi}_0)], \quad (25)$$

that is, the topology derivative is obtained from the expectation of a product comprised of the response function and its topology derivative.

For simplicity, we denote  $D_T y(\Omega, \mathbf{X}, \boldsymbol{\xi}_0)$  by  $z(\Omega, \mathbf{X}, \boldsymbol{\xi}_0)$ , and construct its  $S$ -variate,  $m$ th-order PDD approximation  $\tilde{z}_{S,m}$  as

$$\tilde{z}_{S,m}(\Omega, \mathbf{X}, \boldsymbol{\xi}_0) := z_0(\Omega, \boldsymbol{\xi}_0) + \sum_{\substack{\emptyset \neq u \subseteq \{1, \dots, N\} \\ 1 \leq |u| \leq S}} \sum_{\substack{\mathbf{j}_{|u|} \in \mathbb{N}^{|u|} \\ \|\mathbf{j}_{|u|}\|_\infty \leq m}} D_{u\mathbf{j}_{|u|}}(\Omega, \boldsymbol{\xi}_0) \psi_{u\mathbf{j}_{|u|}}(\mathbf{X}_u; \Omega), \quad (26)$$

Replacing  $y$  and  $D_T y$  of Eq. (25) with their  $S$ -variate,  $m$ th-order PDD approximations  $\tilde{y}_{S,m}$  and  $\tilde{z}_{S,m}$ , respectively, we have

$$D_T \tilde{m}_{S,m}^{(r)}(\Omega, \boldsymbol{\xi}_0) = \mathbb{E} [r \tilde{y}_{S,m}^{r-1}(\Omega, \mathbf{X}) \tilde{z}_{S,m}(\Omega, \mathbf{X}, \boldsymbol{\xi}_0)] \quad (27)$$

For  $r = 1, 2, 3$ , employing the zero mean property and orthonormal property of the PDD basis  $\psi_{u\mathbf{j}_{|u|}}(\mathbf{X}_u; \Omega)$  yields analytical formulations for topology sensitivity of first three moments

$$D_T \tilde{m}_{S,m}^{(1)}(\Omega, \boldsymbol{\xi}_0) = z_0(\Omega, \boldsymbol{\xi}_0), \quad (28)$$

$$D_T \tilde{m}_{S,m}^{(2)}(\Omega, \boldsymbol{\xi}_0) = 2 \times \left[ y_0(\Omega) z_0(\Omega, \boldsymbol{\xi}_0) + \sum_{\substack{\emptyset \neq u \subseteq \{1, \dots, N\} \\ 1 \leq |u| \leq S}} \sum_{\substack{\mathbf{j}_{|u|} \in \mathbb{N}^{|u|} \\ \|\mathbf{j}_{|u|}\|_\infty \leq m}} C_{u\mathbf{j}_{|u|}}(\Omega) D_{u\mathbf{j}_{|u|}}(\Omega, \boldsymbol{\xi}_0) \right], \quad (29)$$

$$D_T \tilde{m}_{S,m}^{(3)}(\Omega, \boldsymbol{\xi}_0) = 3 \times \left[ z_0(\Omega, \boldsymbol{\xi}_0) \tilde{m}_{S,m}^{(2)}(\Omega) + 2y_0(\Omega) \sum_{\substack{\emptyset \neq u \subseteq \{1, \dots, N\} \\ 1 \leq |u| \leq S}} \sum_{\substack{\mathbf{j}_{|u|} \in \mathbb{N}^{|u|} \\ \|\mathbf{j}_{|u|}\|_\infty \leq m}} C_{u\mathbf{j}_{|u|}}(\Omega) D_{u\mathbf{j}_{|u|}}(\Omega, \boldsymbol{\xi}_0) + T_k \right], \quad (30)$$

$$T_k = \sum_{\substack{0 \neq u, v, w \subseteq \{1, \dots, N\} \\ 1 \leq |u|, |v|, |w| \leq S}} \sum_{\substack{\mathbf{j}_{|u|}, \mathbf{j}_{|v|}, \mathbf{j}_{|w|} \in \mathbb{N}^{|\mathbf{j}|} \\ \|\mathbf{j}_{|u|}\|_{\infty}, \|\mathbf{j}_{|v|}\|_{\infty}, \|\mathbf{j}_{|w|}\|_{\infty} \leq m}} C_{u\mathbf{j}_{|u|}}(\Omega) C_{v\mathbf{j}_{|v|}}(\Omega) D_{w\mathbf{j}_{|w|}}(\Omega, \xi_0) \times \\ \mathbb{E}_{\mathbf{d}} \left[ \psi_{u\mathbf{j}_{|u|}}(\mathbf{X}_u; \Omega) \psi_{v\mathbf{j}_{|v|}}(\mathbf{X}_v; \Omega) \psi_{w\mathbf{j}_{|w|}}(\mathbf{X}_w; \Omega) \right], \quad (31)$$

which requires expectations of various products of three random orthonormal polynomials [51]. However, if  $\mathbf{X}$  follows classical distributions such as Gaussian, Exponential, and Uniform distribution, then the expectations are easily determined from the properties of univariate Hermite, Laguerre, and Legendre polynomials [67, 68, 52]. For general distributions, numerical integration methods will apply.

### 4.3. Topology sensitivity of reliability

Using PDD to approximate the performance function  $y$ , the Monte Carlo estimate for topology sensitivity of failure probability is

$$D_T P[\mathbf{X} \in \Omega_{F,k}] \cong \lim_{\rho \rightarrow 0} \frac{1}{\rho^n} \lim_{L \rightarrow \infty} \frac{1}{L} \sum_{l=1}^L \left[ I_{\tilde{\Omega}_{F,k,\rho}}(\mathbf{x}^{(l)}) - I_{\tilde{\Omega}_{F,k}}(\mathbf{x}^{(l)}) \right], \quad (32)$$

where  $L$  is the sample size;  $\mathbf{x}^{(l)}$  is the  $l$ th realization of  $\mathbf{X}$ ;  $I_{\tilde{\Omega}_{F,k}}$  and  $I_{\tilde{\Omega}_{F,k,\rho}}$  are the indicator functions for failure domains  $\tilde{\Omega}_{F,k} := \{\mathbf{x} : \tilde{y}_k(\Omega, \mathbf{x}) < 0\}$  and  $\tilde{\Omega}_{F,k,\rho} := \{\mathbf{x} : \tilde{y}_k(\Omega_\rho, \mathbf{x}) < 0\}$ , respectively. The PDD approximation of the response function of the current topology design  $\Omega$  is  $\tilde{y}_k(\Omega, \mathbf{x})$ , while at perturbed design  $\Omega_\rho$ , it is  $\tilde{y}_k(\Omega_\rho, \mathbf{x})$ . When  $\rho$  takes finite values, Equation (32) leads to a finite-difference approximation

$$D_T P[\mathbf{X} \in \Omega_{F,k}] \cong \frac{1}{\rho^n} \lim_{L \rightarrow \infty} \frac{1}{L} \sum_{l=1}^L \left[ I_{\tilde{\Omega}_{F,k,\rho}}(\mathbf{x}^{(l)}) - I_{\tilde{\Omega}_{F,k}}(\mathbf{x}^{(l)}) \right] \quad (33)$$

of the topology derivative for reliability. It requires  $\tilde{y}_k(\Omega_\rho, \mathbf{X})$ , which is simply obtained from

$$\tilde{y}_k(\Omega_\rho, \mathbf{X}) \cong \tilde{y}_k(\Omega, \mathbf{X}) + \rho^n D_T \tilde{y}_k(\Omega, \mathbf{X}), \quad (34)$$

without additional PDD expansion or FEA involved. This Monte Carlo estimation entails only two PDD approximations, Eq. (5) for the response function itself and Eq. (26) for its deterministic topology derivative, both of which are generated from the same stochastic analysis. Therefore little additional computational cost is needed to evaluate the topology sensitivity of reliability once the stochastic analysis is done, facilitating a novel and highly efficient sensitivity analysis approach for RBTO.

## 5. Calculation of PDD Coefficients

The expansion coefficients in Eq. (5) and Eq. (26) are defined by  $N$ -dimensional integrations  $y_0(\Omega) := \int_{\mathbb{R}^N} y(\mathbf{x}) f_{\mathbf{X}}(\mathbf{x}) d\mathbf{x}$  and  $C_{u\mathbf{j}_{|u|}}(\Omega) := \int_{\mathbb{R}^N} y(\mathbf{x}) \psi_{u\mathbf{j}_{|u|}}(\mathbf{X}_u; \Omega) f_{\mathbf{X}}(\mathbf{x}) d\mathbf{x}$  etc. For large  $N$ , direct numerical integration is often prohibitive, especially when FEA is involved in the Gauss point evaluation. Instead, we will use the dimension-reduction method [23, 69, 24], which entails multiple low-dimensional integrations as an effective replacement of a single  $N$ -dimensional integration.

Let  $\mathbf{c} = (c_1, \dots, c_N)^T \in \mathbb{R}^N$ , which is commonly adopted as the mean of  $\mathbf{X}$ , be a reference point, and  $y(\mathbf{x}_v, \mathbf{c}_{-v})$  represent an  $|v|$ -variate referential dimensional decomposition (RDD) component function of  $y(\mathbf{X})$ , where  $v \subseteq \{1, \dots, N\}$  and  $-v = \{1, \dots, N\} \setminus v$ . Given a positive integer  $S \leq R \leq N$ , when  $y(\mathbf{x})$  in the above  $N$ -dimensional integration is replaced by its  $R$ -variate RDD approximation, the coefficients are estimated from [23]

$$y_0(\Omega) \cong \sum_{i=0}^R (-1)^i \binom{N-R+i-1}{i} \sum_{\substack{v \subseteq \{1, \dots, N\} \\ |v|=R-i}} \int_{\mathbb{R}^{|v|}} y(\mathbf{x}_v, \mathbf{c}_{-v}) f_{\mathbf{X}_v}(\mathbf{x}_v) d\mathbf{x}_v \quad (35)$$

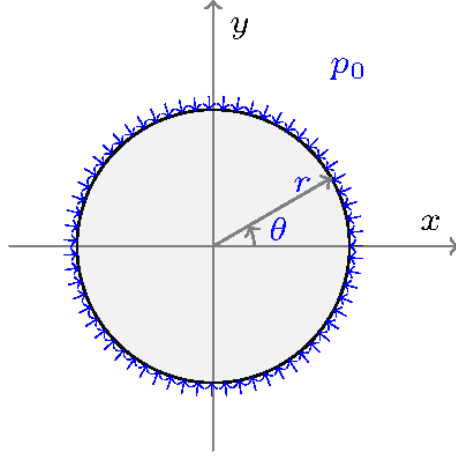


Figure 2: A round disk subject to a uniform pressure

$$C_{u_j|u_i}(\Omega) \cong \sum_{i=0}^R (-1)^i \binom{N-R+i-1}{i} \sum_{\substack{v \subseteq \{1, \dots, N\} \\ |v|=R-i, u \subseteq v}} \int_{\mathbb{R}^{|v|}} y(\mathbf{x}_v, \mathbf{c}_{-v}) \psi_{u_j|u_i}(\mathbf{x}_u; \Omega) f_{\mathbf{x}_v}(\mathbf{x}_v) d\mathbf{x}_v \quad (36)$$

entailing at most  $R$ -dimensional integrations. For each integration involved, the Gauss quadrature rule applies. For engineering problems, the evaluation of Gauss points often relies on FEA. For instance, each FEA with  $\mathbf{X}$  realized at certain gauss point supplies response function value for that Gauss point. Whereas to approximate the coefficients for the topology sensitivity  $D_T y(\Omega, \mathbf{X}, \xi_0)$  or  $z(\Omega, \mathbf{X}, \xi_0)$  in section 4.2, each FEA provides stress results for Eq. 24 and further produces  $z$  values at the corresponding Gauss point. Nonetheless the reduced integration is significantly more efficient than performing one  $N$ -dimensional integration owing to a much fewer number of Gauss points required by the former, particularly when  $R \ll N$ . Moreover, it facilitates the calculation of coefficients approaching their exact value as  $R \rightarrow N$ . In addition, the same set of Gauss points thus the same set of FEAs will be reused for the evaluation of coefficients in Eq. (26), rendering a significantly efficient framework for stochastic topology sensitivity analysis.

## 6. Numerical Examples

In this section, two new benchmark examples are developed for the analytical or semi-analytical solution of moments and reliability and their topology sensitivities. The first one involves two random variables and renders analytical expression for both stochastic quantities and their topology sensitivities of compliance. The second one contains 53 random variables to test the accuracy and efficiency of the proposed method for high dimensional problems by developing corresponding analytical and semi-analytical solutions. The third example is a three-dimensional bracket, whose topology has already been optimized, illustrating a practical application of the proposed method. In all examples, orthonormal polynomials and associated Gauss quadrature rules consistent with the probability distributions of input variables, including classical forms, if they exist, were employed. No unit for length, force, and Young's modulus is specified in all examples for simplicity while permitting any consistent unit system for the results.

### 6.1. A round disk subject to a uniform pressure

Assuming the plane stress state, consider a round disk  $\Omega = \{(r, \theta) : r \leq 1, \theta \in [0, 2\pi)\}$  subject to a uniform pressure  $p_0$  as shown in Fig. 2, where  $(r, \theta)$  is the polar coordinate system with its origin locating at the center of the disk. The Young's module  $E$  and pressure  $p_0$  are random variables. The Poisson's ratio  $\nu = 0.2$ , and is deterministic.

Assume  $E$  follows inverse uniform distribution on  $[2, 4]$  with the probability density function (PDF)

$$f_E(x_E) = 4x_E^{-2} \quad (37)$$

Table 2: Analytical solutions, numerical results, and relative errors: moments

	$m^{(1)}$		$m^{(2)}$		$m^{(3)}$	
	values	Relative Error (%)	values	Relative Error (%)	values	Relative Error (%)
PDD $S = 1, m = 1$	4.387142651	0.252	22.31764876	2.308	124.853276	7.523
PDD $S = 1, m = 2$	4.392067155	0.140	22.43673535	1.786	127.987972	5.201
PDD $S = 1, m = 3$	4.392213984	0.137	22.44094545	1.768	128.078790	5.134
PDD $S = 2, m = 1$	4.392955528	0.120	22.69742049	0.645	131.939662	2.274
PDD $S = 2, m = 2$	4.398062552	0.004	22.83944821	0.024	136.197391	0.879
PDD $S = 2, m = 3$	4.398214737	$3.4 \times 10^{-4}$	22.84455042	$1.3 \times 10^{-3}$	136.337101	0.983
Analytical	$\frac{7\pi}{4}(1-\nu)$		$\frac{217\pi^2}{60}(1-\nu)^2$		$\frac{1905\pi^3}{224}(1-\nu)^3$	

and  $P_0$  follows uniform distribution on  $[1, 2]$ . For this particular problem, the exact compliance is readily available, it is

$$y(\Omega) = 2\pi \frac{1-\nu}{E} p_0^2. \quad (38)$$

The exact PDF of the compliance for this particular problem is found as

$$f_Y(y) = \begin{cases} \frac{1}{\pi(1-\nu)} \left( 2 - \left( \frac{y}{2\pi(1-\nu)} \right)^{-\frac{1}{2}} \right) & \frac{\pi(1-\nu)}{2} \leq y < \pi(1-\nu) \\ \frac{1}{\pi(1-\nu)} \left( \frac{y}{2\pi(1-\nu)} \right)^{-\frac{1}{2}} (\sqrt{2} - 1) & \pi(1-\nu) \leq y < 2\pi(1-\nu) \\ \frac{1}{\pi(1-\nu)} \left( \sqrt{2} \left( \frac{y}{2\pi(1-\nu)} \right)^{-\frac{1}{2}} - 1 \right) & 2\pi(1-\nu) \leq y < 4\pi(1-\nu) \end{cases}. \quad (39)$$

Moreover, the analytical expression of the first three moments of compliance are summarized in the Table 2

To calculate the analytical topology sensitivity of moments and failure probability at the center  $\xi_0$ , another analytical solution for the perforated domain with a tiny hole at the center is needed. It reads

$$y(\Omega_\rho) = \frac{2\pi p_0^2}{E(1-\rho^2)} \left[ (1+\nu)\rho^2 + (1-\nu) \right], \quad (40)$$

which can be derived based on the *Lamé's strain potential*  $C \ln \frac{r}{K}$  with undetermined constants  $C$  and  $K$  via the displacement method. The deterministic topology derivative  $D_T y$  by definition is

$$D_T y(\Omega, \xi_0) = \lim_{\epsilon \rightarrow 0} \frac{y(\Omega_\rho) - y(\Omega)}{\rho^2} = \frac{4\pi p_0^2}{E}. \quad (41)$$

Together with Eqs. (25) and (39), the analytical expressions of topology sensitivity for the first three moments can be determined, and are listed in Table 3.

The finite element model employed in the proposed method consists of 404800 quadrilateral and 1600 triangular elements. The displacement  $u_\theta$  at  $(1, 0)$ ,  $(1, \frac{\pi}{2})$ , and  $(1, \frac{3\pi}{2})$ , are specified as *zero* to make the FEA model well-posed and keep the same solution of stress, strain, and compliance in Fig. 2. Table 2 displays the approximate moments of the compliance, committed by the proposed univariate ( $S = 1$ ) and bivariate ( $S = 2$ ) PDD for  $m = 1, 2, 3$ . Relative errors, defined as the ratio of the absolute error to the exact value, are also presented. For the first moments, the errors range from  $3.4 \times 10^{-4}$  to 0.252 percent. When the order of moments increases, the errors show an uptrend as expected due to the accumulation of approximation errors, but still maintains good levels,  $1.3 \times 10^{-3}$  to 2.308 percent for the second moments and 0.983 to 7.523 percent for the third moments.

Table 3 presents the approximate topology sensitivity of the center point and their relative errors for the first three moments. For the same set of  $S$  and  $m$  values, the relative errors of topology sensitivity are almost identical with the ones of moments in Table 2. It seems unusual since for many methods the numerical estimation of stochastic sensitivity is often less accurate than the estimation of the function itself. However, the proposed method dovetails the deterministic topology derivative  $D_T y$  as shown in Eq. (25) and the nonlinearity and interactive effects in  $D_T y$  are

Table 3: Analytical solutions, numerical results, and relative errors: sensitivity of moments at  $\xi_0 = (0, 0)$ 

	$D_T m^{(1)}(\Omega, \xi_0)$		$D_T m^{(2)}(\Omega, \xi_0)$		$D_T m^{(3)}(\Omega, \xi_0)$	
	values	Relative Error (%)	values	Relative Error (%)	values	Relative Error (%)
PDD $S = 1, m = 1$	10.96790142	0.252	111.5886904	2.307	936.4032737	7.522
PDD $S = 1, m = 2$	10.98019122	0.140	112.1839012	1.786	959.9116087	5.201
PDD $S = 1, m = 3$	10.98056234	0.137	112.2050067	1.768	960.5932965	5.134
PDD $S = 2, m = 1$	10.98243457	0.120	113.4875794	0.645	989.5516625	2.274
PDD $S = 2, m = 2$	10.99517968	0.004	114.1974516	0.023	1021.481992	0.879
PDD $S = 2, m = 3$	10.99556439	$9.0 \times 10^{-5}$	114.2230294	$1.0 \times 10^{-3}$	1022.530638	0.983
Analytical	$\frac{7\pi}{2}$		$\frac{217\pi^2}{15}(1-\nu)$		$\frac{5715\pi^3}{112}(1-\nu)^2$	

Table 4: comparison between analytical solution and numerical results: reliability and its sensitivity for  $\rho = 0.05, \bar{y} = 7.0$  at  $\xi_0 = (0, 0)$ 

	$P_F := P(y \geq \bar{y}), \bar{y} = 7.0$		$D_T P_F(\Omega, \xi_0)$	
	values	Relative Error (%)	values	Relative Error (%)
PDD $S = 1, m = 1$	$0.72325 \times 10^{-1}$	34.028	1.9776	43.154
PDD $S = 1, m = 2$	$0.85563 \times 10^{-1}$	21.953	1.6684	20.772
PDD $S = 1, m = 3$	$0.85065 \times 10^{-1}$	22.407	1.6516	19.556
PDD $S = 2, m = 1$	0.105089	4.142	1.6744	21.206
PDD $S = 2, m = 2$	0.110683	0.9602	1.3936	0.8797
PDD $S = 2, m = 3$	0.109681	0.04622	1.4284	3.3988
Analytical( $\rho \rightarrow 0$ )	$1 - \frac{4\sqrt{5.6\pi-2.4\pi-7}}{0.8\pi}$		$\frac{4\sqrt{5.6\pi-14}}{0.64\pi}$	

often similar with the response  $y$  as shown in Eqs (38) and (41), which lead to similar or identical relative errors in the sensitivity of moments. The errors from the propose method drop as  $m$  and  $S$  increase as expected for both moments and their topology sensitivities.

Analytical expressions and numerical results of failure probabilities and their topology sensitivity are presented in Tables 4 and 5 for two limit-state values 7.0 and 7.5, respectively. The numerical estimations of failure probability by the proposed method are evaluated via Eq. (12) using the embedded MCS, whereas their topology sensitivities are calculated based on Eqs. (33) and (34) with a finite  $\rho$  value of 0.05. The sample size for both is  $L = 10^6$ . The total number of FEA simulations for various combinations of the truncation parameters  $S = 1, 2$  and  $m = 1, 2, 3$  are listed in the Table 5. It is worthy to note that one set of FEAs generate the associated PDD approximations for both the response function and its deterministic topology derivatives at the same time. In addition, the two PDD approximations deliver stochastic analyses and stochastic topology sensitivity analyses, generating moments, reliabilities, and their topology sensitivities without additional FEAs. The errors of failure probability and its sensitivity by the linear ( $m = 1$ ) univariate ( $S = 1$ ) PDD are relatively large, but it requires only 5 FEAs. But the errors drop significantly as  $S$  and/or  $m$  increases. For instance, the errors of failure probability become less than one percent for  $S = 2, m = 2, 3$ , requiring 15 and 25 FEAs respectively. Similar trends are observed in their topology sensitivity. Comparing results for  $\bar{y} = 7.0$  and  $\bar{y} = 7.5$ , the errors of failure probability increase as expected when the limit state values move away from the mean of the response function. Further developments address this problem in our future work.

## 6.2. A 53-random-variable example: the round disk subject to pressure in terms of trigonometric functions

Consider the same round disk in last example but subject to a more complex pressure as shown in Fig. 3, where the pressure function

$$f(\theta) = D_0 + \sum_{k=1}^K (D_k \cos(k+1)\theta + E_k \sin(k+1)\theta) \quad (42)$$

accommodating  $2K + 1$  random variables  $D_k, k = 0, \dots, K$  and  $E_k, k = 1, \dots, K$ .

Table 5: comparison between analytical solution and numerical results: reliability and its sensitivity for  $\rho = 0.05, \bar{y} = 7.5$  at  $\xi_0 = (0, 0)$

	$P_F := P(y \geq \bar{y}), \bar{y} = 7.5$		$D_T P_F(\Omega, \xi_0)$		# of FEA
	values	Relative Error (%)	values	Relative Error (%)	
PDD $S = 1, m = 1$	$0.26411 \times 10^{-1}$	64.440	1.3572	15.313	5
PDD $S = 1, m = 2$	$0.44418 \times 10^{-1}$	40.196	1.3540	15.041	5
PDD $S = 1, m = 3$	$0.44335 \times 10^{-1}$	40.307	1.3052	10.895	9
PDD $S = 2, m = 1$	$0.62140 \times 10^{-1}$	16.335	1.4212	20.751	9
PDD $S = 2, m = 2$	$0.749340 \times 10^{-1}$	0.8911	1.1672	0.8297	15
PDD $S = 2, m = 3$	$0.741870 \times 10^{-1}$	0.1147	1.1748	0.1840	25
Analytical( $\rho \rightarrow 0$ )	$1 - \frac{4\sqrt{6\pi-2.4\pi-7.5}}{0.8\pi}$		$\frac{4\sqrt{6\pi-15}}{0.64\pi}$		NA

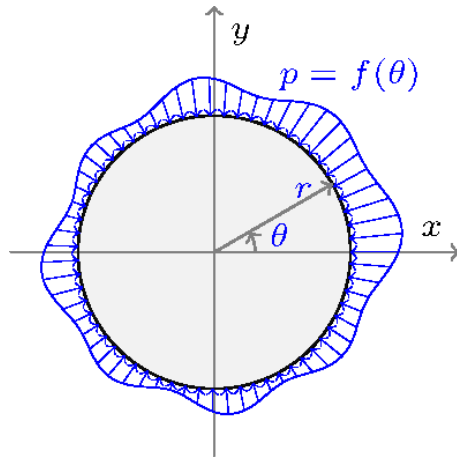


Figure 3: A round disk subject to a complex pressure

### 6.2.1. Analytical solutions

Employing the *Taylor series expansion* of holomorphic functions in a simply-connected domain and *Goursat formula* [70], the analytical solution for compliance of the disk subject to the above pressure is found in the form of

$$y(\Omega) = \frac{2D_0^2\pi(1-\nu)}{E} + \sum_{k=1}^K \frac{(D_k^2 + E_k^2)\pi(\nu + 2k + 1)}{k(k+2)E}. \quad (43)$$

The solution (43) is general and applicable for the pressure function (42) for any positive integer  $K$ .

Now consider perforating a tiny hole of radius  $\rho$  in the center of the disk. Its compliance, subject to the same pressure function (42), is found as follows

$$y(\Omega_\rho) = \frac{2D_0^2\pi[\rho^2(1+\nu) + (1-\nu)]}{E(1-\rho^2)} + \sum_{k=1}^K \frac{A_k B_k}{C_k F_k}, \quad (44)$$

where

$$A_k = (D_k^2 + E_k^2)\pi$$

$$B_k = \rho^{2k}(k+2)[k\nu - (3k+2) - (k\nu + k+2)\rho^2] + [(\nu - 2k - 3)\rho^{2(k+2)} - (\nu + 2k + 1)] \sum_{j=0}^{k-1} \rho^{2j}$$

$$C_k = k(k+2)E$$

$$F_k = k(k+2)\rho^{2k}(1-\rho^2) + (\rho^{2(k+2)} - 1) \sum_{j=0}^{k-1} \rho^{2j}.$$

which requires *Laurent series expansion* of holomorphic functions in a double-connected region.

Employing Eqs. (43) and (44), the analytical expression of the deterministic topology derivative at the center reads

$$D_T y(\Omega, \xi_0) = \lim_{\rho \rightarrow 0} \frac{y(\Omega_\rho) - y(\Omega)}{\rho^2} = \frac{4\pi(D_0^2 + 2D_1^2 + 2E_1^2)}{E}, \quad (45)$$

indicating that at the center of the disk the topology derivative of compliance is merely related to Young's modulus  $E$  and three parameters  $D_0, D_1, E_1$  in the pressure function.

The exact topological sensitivities of moments at the center are derived from

$$D_T m^{(r)}(\Omega, \xi_0) = \int_{\mathbb{R}^N} r y^{r-1}(\Omega, \mathbf{X}) D_T y(\Omega, \mathbf{X}, \xi_0) f_{\mathbf{X}}(\mathbf{x}) d\mathbf{x}, \quad (46)$$

employing Eqs. (43) and (45). Generally, Eq. (46) admits any proper distributions for the  $2K + 1$  random variables.

### 6.2.2. Benchmarks

Let  $K = 25$ , random variables  $D_k, k = 0, \dots, 25$  and  $E_k, k = 1, \dots, 25$  follow four-parameter Beta distributions with mean value  $\mu_{D_k} = k + 1, \mu_{E_k} = k + 1$ , and coefficient of variance (CV) be 0.1 for all  $D_k$  and  $E_k$ . Two isotropic elastic material constants also follow four-parameter Beta distributions, where Young's modulus  $E$  has a mean value of  $10^6$  and CV of 0.1, the Poisson's ratio  $\nu$  has a mean value of 0.2 and CV of 0.01. The support of each Beta variable is  $[\mu - 3\sigma, \mu + 3\sigma]$ , where  $\mu$  and  $\sigma$  here denote mean and standard deviation of the corresponding variable.

The exact solutions of the first three moments of the compliance, obtained based on the analytical solution (43), are exhibited in Table 6. For the finite element model used in the proposed method, two types of mesh are adopted: 1) coarse mesh (24800 quadrilateral and 400 triangular elements), and 2) fine mesh (404800 quadrilateral and 1600 triangular elements), as shown in Tables 6 and 7. The displacement  $u_\theta$  at  $(1, 0), (1, \frac{\pi}{2}),$  and  $(1, \frac{3\pi}{2})$ , are specified as *zero* to make the FEA model well-posed and meanwhile keep the compliance unchanged. For the results by the coarse mesh, the relative errors of the first moment by the proposed method with various truncations range from 1.056 to



Table 6: Exact solutions, numerical results, and relative errors for moments - coarse mesh

	$m^{(1)}$		$m^{(2)}$		$m^{(3)}$	
	values	Relative Error (%)	values	Relative Error (%)	values	Relative Error (%)
PDD $S = 1, m = 1$	4.35037888E-3	1.146	1.90933140E-5	2.532	8.452068041E-8	4.183
PDD $S = 1, m = 2$	4.35088784E-3	1.134	1.91037093E-5	2.479	8.46574593E-8	4.028
PDD $S = 1, m = 3$	4.35081912E-3	1.136	1.91032666E-5	2.481	8.46571311E-8	4.029
PDD $S = 2, m = 1$	4.35332715E-3	1.079	1.91218647E-5	2.386	8.47307023E-8	3.945
PDD $S = 2, m = 2$	4.35171366E-3	1.116	1.91138791E-5	2.427	8.47479823E-8	3.926
PDD $S = 2, m = 3$	4.35436004E-3	1.056	1.91370811E-5	2.308	8.49035726E-8	3.749
Exact	4.400814209E-3		1.958928121E-5		8.821066188E-8	

1.146 percent. When the order of moments increases, the relative errors rise, for instance, to 2.308-2.532 percent for the second moment and to 3.749-4.183 percent for the third moment. This trend is foreseeable since the moment calculation accumulates the error of the approximated response function when its order increases. Checking any particular moment in Table 6, the prevailing trend of the relative errors is down when increasing truncation parameters  $S$  and  $m$ , but it is insignificant. The reason as disclosed in the later discussion is that the error introduced by FEA approximations is dominant comparing to the error of the PDD approximation. Nonetheless, roughly 1.1 percent error for  $m^{(1)}$ , 2.4 percent error for  $m^{(2)}$ , and 4.0 percent error for  $m^{(3)}$  are highly satisfactory for stochastic moment analysis using the coarse mesh. When employing the fine mesh, the relative errors of all three moments plummet approximately by half for every combination of truncation parameters as shown in Table 7, which indicates the error from FEA may dominate the error of PDD approximations. The relative errors for  $m^{(1)}$ ,  $m^{(2)}$ , and  $m^{(3)}$  by the proposed method using the fine mesh are merely 0.4, 1.1, and 2.0 percent, respectively.

The topology sensitivities for the first three moments of compliance are examined at the center point  $\xi_0 = (0, 0)$ , indicating the change ratio of the three moments after perforating a tiny hole at  $\xi_0$ . Their exact solutions are unveiled in Tables 8 and 9. The proposed method is implemented in all combinations of  $S = 1, 2$  and  $m = 1, 2, 3$  for various PDD truncations and the corresponding results by coarse and fine mesh are listed in Tables 8 and 9, respectively. It is noteworthy that the proposed method for topology sensitivity of moments roots in Eqs. (28)-(30), which dovetail PDD approximation of the deterministic topology derivative of the response. The ranges of relative errors for the topology sensitivities by the proposed method are [0.066, 0.422], [1.168, 1.800], and [2.614, 3.444] when using the coarse mesh. Whereas using the fine mesh, they are [0.193, 0.389], [0.808, 1.058], and [1.627, 2.011], respectively, showing significant drops especially in the errors of  $D_T m^{(2)}(\Omega, \xi_0)$  and  $D_T m^{(3)}(\Omega, \xi_0)$ . Tables 6-9 demonstrate that the proposed method is capable of performing highly accurate moment analysis as well as their topology sensitivity analysis. By comparing results from two mesh cases, it can be inferred that a significant portion of errors come from FEA, conjointly evincing the accuracy of the proposed method. Moreover, sensitivity analyses not limited to topology sensitivity analyses of a generic response function are often less accurate than the evaluation of the function itself. However, comparing Table 6 with Table 8, or Table 7 with Table 9, it shows that for the same mesh case and the same set of  $S$  and  $m$  the topology sensitivity is surprisingly more accurate than the moment analysis itself. For instance, 1.800 percent error for  $D_T m^{(2)}(\Omega, \xi_0)$  is less than 2.532 percent error for  $m^{(2)}$  itself in the case of coarse mesh,  $S = 1$ , and  $m = 1$ . The remarkable more accuracy of sensitivity seems occasional and rare, however, it is reasonable for the proposed framework due to the deterministic topology embedded in Eqs. (25)-(30). Scrutinizing the definition of the  $r$ th moment  $m^{(r)}(\Omega) := \mathbb{E}[y^r(\Omega, \mathbf{X})]$  and its topology sensitivity Eq. (25), a major difference between them is the replacement of  $y$  by  $D_T y$  in the topology sensitivity. When the nonlinearity and interaction structure of  $D_T y$  is equal or simpler than ones of  $y$ , for the same set of truncation parameter  $S$  and  $m$ , the topology sensitivity of moments calculated by the proposed method is bound to be equally or more accurate than the moments itself. The deterministic topology derivative at the center for this example is shown in Eq. (45), which is obviously simpler than the compliance itself as shown in Eq. (43). The structure of the proposed method in Eqs. (25)-(30) well explains the observation that topology sensitivity is more accurate than the moment itself and also demonstrates another advantage of the new method.

For failure probability and its topology sensitivity, analytical expressions or exact values are not readily available

Table 7: Exact solutions, numerical results, and relative errors for moments - fine mesh

	$m^{(1)}$		$m^{(2)}$		$m^{(3)}$	
	values	Relative Error (%)	values	Relative Error (%)	values	Relative Error (%)
PDD $S = 1, m = 1$	4.38180775E-3	0.432	1.93702207E-5	1.118	8.63662287E-8	2.091
PDD $S = 1, m = 2$	4.38225397E-3	0.422	1.93801836E-5	1.067	8.65021250E-8	1.937
PDD $S = 1, m = 3$	4.38226696E-3	0.421	1.93804554E-5	1.066	8.65065744E-8	1.932
PDD $S = 2, m = 1$	4.38201078E-3	0.427	1.93749344E-5	1.094	8.64199812E-8	2.030
PDD $S = 2, m = 2$	4.38253889E-3	0.415	1.93857124E-5	1.039	8.65628909E-8	1.868
PDD $S = 2, m = 3$	4.38229842E-3	0.421	1.93837562E-5	1.049	8.65525631E-8	1.880
Exact	4.400814209E-3		1.958928121E-5		8.821066188E-8	

Table 8: Exact solutions, numerical results, and relative errors for sensitivities of moments at  $\xi_0 = (0, 0)$  - coarse mesh

	$D_T m^{(1)}(\Omega, \xi_0)$		$D_T m^{(2)}(\Omega, \xi_0)$		$D_T m^{(3)}(\Omega, \xi_0)$	
	values	Relative Error (%)	values	Relative Error (%)	values	Relative Error (%)
PDD $S = 1, m = 1$	2.17057140E-4	0.422	1.90394853E-6	1.800	1.26338374E-8	3.444
PDD $S = 1, m = 2$	2.17096271E-4	0.404	1.90509883E-6	1.741	1.26550116E-8	3.282
PDD $S = 1, m = 3$	2.17074018E-4	0.414	1.90489284E-6	1.752	1.26538907E-8	3.291
PDD $S = 2, m = 1$	2.17834040E-4	0.066	1.91224312E-6	1.372	1.27006070E-8	2.934
PDD $S = 2, m = 2$	2.17282453E-4	0.319	1.90734319E-6	1.625	1.26761294E-8	3.121
PDD $S = 2, m = 3$	2.18166027E-4	0.087	1.91619922E-6	1.168	1.27424908E-8	2.614
Exact	2.179771038E-4		1.938851314E-6		1.308450116E-8	

Table 9: Exact solutions, numerical results, and relative errors for sensitivities of moments at  $\xi_0 = (0, 0)$  - fine mesh

	$D_T m^{(1)}(\Omega, \xi_0)$		$D_T m^{(2)}(\Omega, \xi_0)$		$D_T m^{(3)}(\Omega, \xi_0)$	
	values	Relative Error (%)	values	Relative Error (%)	values	Relative Error (%)
PDD $S = 1, m = 1$	2.17130315E-4	0.389	1.91834626E-6	1.058	1.28213357E-8	2.011
PDD $S = 1, m = 2$	2.17156561E-4	0.376	1.91936534E-6	1.005	1.28417041E-8	1.856
PDD $S = 1, m = 3$	2.17147692E-4	0.381	1.91930875E-6	1.008	1.28418034E-8	1.855
PDD $S = 2, m = 1$	2.17245778E-4	0.336	1.91970278E-6	0.988	1.28347047E-8	1.909
PDD $S = 2, m = 2$	2.17177686E-4	0.367	1.91993928E-6	0.975	1.28503641E-8	1.789
PDD $S = 2, m = 3$	2.17557373E-4	0.193	1.92318241E-6	0.808	1.28716567E-8	1.627
Exact	2.179771038E-4		1.938851314E-6		1.308450116E-8	

Table 10: Benchmark of reliability and its sensitivity for  $\rho = 0.05, \bar{y} = 0.0036$  at  $\xi_0 = (0, 0)$  - coarse mesh

	$P_F := P(y \leq \bar{y}), \bar{y} = 0.0036$		$D_T P_F(\Omega, \xi_0)$		# of FEA
	values	Relative Error (%)	values	Relative Error (%)	
PDD $S = 1, m = 1$ †	4.86690000E-2	127.015	-4.20000000E-2	15.170	107
PDD $S = 1, m = 2$	2.70290000E-2	26.076	-4.12000000E-2	12.976	107
PDD $S = 1, m = 3$	3.02560000E-2	41.128	-3.88000000E-2	6.395	213
PDD $S = 2, m = 1$	4.77570000E-2	122.761	-5.28000000E-2	44.785	5619
PDD $S = 2, m = 2$	2.55110000E-2	18.995	-4.92000000E-2	34.912	11131
PDD $S = 2, m = 3$	2.79250000E-2	30.255	-3.96000000E-2	8.588	22261
Crude MCS-FD‡	2.143872200E-2		-3.646800000E-02		NA

† The sample size for results by proposed method is  $L = 10^6$ ‡ The sample size for the Crude MCS-FD is  $L = 10^9$

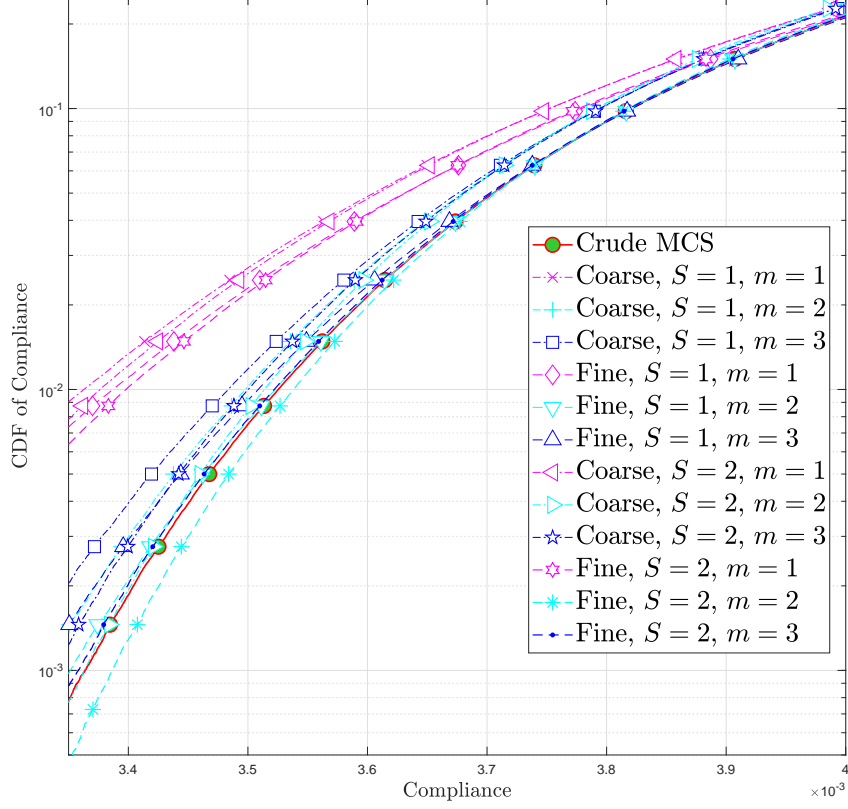


Figure 4: CDF of the compliance

Table 11: Benchmark of reliability and its sensitivity for  $\rho = 0.05, \bar{y} = 0.0036$  at  $\xi_0 = (0, 0)$  - fine mesh

	$P_F := P(y \leq \bar{y}), \bar{y} = 0.0036$		$D_T P_F(\Omega, \xi_0)$		# of FEA
	values	Relative Error (%)	values	Relative Error (%)	
PDD $S = 1, m = 1$ †	4.21980000E-2	96.831	-4.20000000E-2	15.170	107
PDD $S = 1, m = 2$	2.17680000E-2	1.536	-3.48000000E-2	4.574	107
PDD $S = 1, m = 3$	2.45970000E-2	14.732	-3.36000000E-2	7.864	213
PDD $S = 2, m = 1$	4.18240000E-2	95.086	-4.72000000E-2	29.429	5619
PDD $S = 2, m = 2$	1.99170000E-2	7.098	-3.76000000E-2	3.104	11131
PDD $S = 2, m = 3$	2.30350000E-2	7.446	-3.60000000E-2	1.283	22261
Crude MCS-FD‡	2.143872200E-2		-3.646800000E-2		NA

† The sample size for results by the proposed method is  $L = 10^6$

‡ The sample size for the Crude MCS-FD is  $L = 10^9$

for this example. For simplicity, the crude MCS that employs the analytical compliance Eq. (43) and a sample size  $L = 10^9$  is taken as the benchmark solution of failure probability. Meanwhile, a finite difference formulation embedded the crude MCS (Crude MCS-FD)

$$D_T P [\mathbf{X} \in \Omega_F] \cong \frac{1}{\rho^n} \lim_{L \rightarrow \infty} \frac{1}{L} \sum_{l=1}^L [I_{\Omega_{F,\rho}}(\mathbf{x}^{(l)}) - I_{\Omega_F}(\mathbf{x}^{(l)})] \quad (47)$$

is adopted as the benchmark solution of topology sensitivity of failure probability, where the radius of the perforated hole takes a finite value  $\rho = 0.05$ , the sample size  $L = 10^9$ ,  $I_{\Omega_F}$  and  $I_{\Omega_{F,\rho}}$  are the indicator functions of the exact failure domains  $\Omega_F := \{\mathbf{x} : y(\Omega, \mathbf{x}) < \bar{y}\}$  and  $\Omega_{F,\rho} := \{\mathbf{x} : y(\Omega_\rho, \mathbf{x}) < \bar{y}\}$  with  $y(\Omega, \mathbf{x})$  taking the exact compliance function of the disk as shown in Eq. (43) and  $y(\Omega_\rho, \mathbf{x})$  taking the exact compliance function of the perforated disk as shown in Eq. (44). These benchmark solutions, involving analytical expressions of compliance, MCS, and the finite-difference method, is also referred to as semi-analytical solutions in this paper.

The cumulative distribution function (CDF) of the compliance by crude MCS as well as ones by the proposed method employing two mesh cases and various PDD truncations are plotted in Fig. 4. An identical sample size  $L = 10^6$  is used for all plots in this figure. All the CDF curves spontaneously group into two bundles. The first bundle consists of all linear ( $m = 1$ ) approximations whether univariate ( $S = 1$ ) or bivariate ( $S = 2$ ), fine mesh or coarse mesh. It has considerable errors when comparing with the CDF of crude MCS, indicating that the error due to lack of nonlinearity in the PDD dominants the error from FEA and interactions between random variables. The second bundle includes all the cases of  $m \geq 2$  and provide better approximations. Among them, the cases using fine mesh provide better solutions than coarse mesh ones. The best results are achieved by two fine mesh cases -  $S = 1, m = 2$  and  $S = 2, m = 3$ , and their curves are almost coincide with the one by the crude MCS. Nonetheless, an overall trend of convergence can be roughly observed in Fig. 4 as increasing  $S$  and  $m$  and adopting finer mesh. More quantitative verifications of failure probability and its topology sensitivity are displayed in Tables 10 and 11, in which the failure probability at 0.0036 and its topology sensitivity are evaluated by the proposed method and the crude MCS. The failure probability by the linear approximations ( $m = 1$ ) carries the largest errors among their same-variate and same-mesh counterparts, specifically 127.015 and 122.761 percent for coarse mesh  $S = 1, 2$ , 96.831 and 95.086 percent for fine mesh  $S = 1, 2$ . After increasing  $m$ , the errors plummet dramatically to about 19-41 percent for coarse mesh cases and 2-14 percent for fine mesh cases. The significant differences in error levels of two mesh types imply that the error from FEA predominates in those cases. Similar behaviors are observed in the results of its topology sensitivity but the level of errors have slight or moderate drops for most of  $m \geq 2$  cases. The proposed method with the fine mesh and nonlinearity ( $m \geq 2$ ) provides satisfactory evaluation for the topology sensitivity of failure probability, merely 5-8 percent for univariate and 1-3 percent for bivariate as shown in Table 11. For both failure probability and its sensitivity, Table 10-11 show that the error level roughly drops when increasing  $S$  and  $m$ , but the trend is not monotonic because of the synthetic effect of four kinds of error sources - finite difference, MCS, PDD, and FEA. The number of FEAs required by the proposed method for each PDD truncation is also listed in Table 10-11. Univariate cases are much more efficient than bivariate ones as expected, involving only 107 and 213 FEAs to level down the errors to 1.536 and 14.732 percent in failure probability and 4.574 and 7.864 in its topology sensitivity for fine mesh and  $m = 2, 3$ . It is noteworthy that the same set of FEAs can be used to generate estimations for not only failure probability and its sensitivity but also moments and their sensitivity in preceding tables.

To sum up, this example is constructed to gauge the accuracy of new or existing methods for stochastic analyses and their topology sensitivities by analytical or semi-analytical solutions developed. Although  $K = 25$  is specified, the analytical and semi-analytical solutions developed can be directly used or easily expanded for any positive  $K$  to accommodate even more random variables. Nonetheless, the proposed method is capable of evaluating moments and their sensitivities in a highly accurate manner even using low-variate low-order approximation. For failure probability and its sensitivity, it is also feasible to provide satisfactory evaluations using low-variate but nonlinear approximation. The least number of FEAs required for those fine approximations is 107 for this 53 random variable example, demonstrating the high efficiency of the proposed method for high-dimensional stochastic topology sensitivity analysis. Another advantage of the proposed method observed in this example is its capability of providing higher accuracy in topology sensitivity than in stochastic quantities themselves.

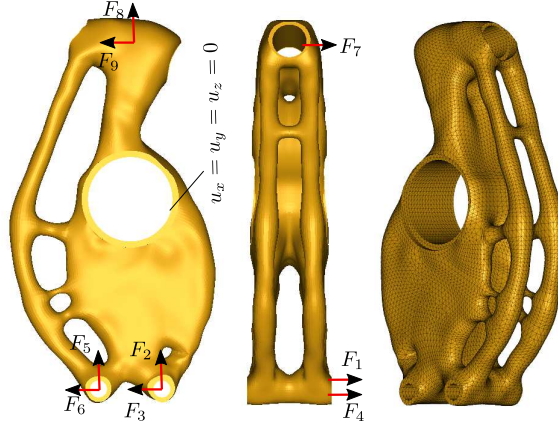


Figure 5: Geometry and mesh of the bracket

### 6.3. An engineering bracket involving 11 random variables

Last, the proposed method is applied to a three-dimensional engineering bracket [71] shown in Fig. 5. With the fixed support at the middle hole, the bracket is subject to nine random tractions along  $x$ ,  $y$ , or  $z$ -direction on the surfaces of one top hole and two bottom holes as shown in Fig. 5. Their mean values are  $(\mu_{F_1}, \mu_{F_2}, \dots, \mu_{F_9}) = (2500.0, 4200.0, -6400.0, 3600.0, -5000.0, -6000.0, -4800.0, 8100.0, -7000.0)$ , respectively. The Young's modulus and Poisson's ratio are also random with mean values  $\mu_E = 2.1 \times 10^9$  and  $\mu_\nu = 0.3$ . The CV for all 11 random variables is 0.1. In this example, all 11 random variables follow truncated Gaussian distribution, which has the following PDF in general

$$f_X(x) = \begin{cases} \frac{1}{\Phi(D) - \Phi(-D)} \phi\left(\frac{x-\mu}{\sigma}\right) & \alpha \leq x \leq \beta, \\ 0 & \text{otherwise,} \end{cases} \quad (48)$$

where  $\mu$  and  $\sigma$  denote the mean and standard deviation of each variable before the truncation and  $\alpha = \mu - D$ ,  $\beta = \mu + D$ . For nine random tractions and Young's modulus,  $D$  takes 10 times of the corresponding standard deviation, that is,  $D = 10\sigma$ . For the random Poisson's ratio,  $D$  takes six times of the corresponding standard deviation to avoid unrealistic materials.

The second-order univariate PDD ( $S = 1, m = 2$ ) is used to perform stochastic topology sensitivity analysis. The finite element model required contains 182540 quadratic tetrahedron elements. Compliance is selected as the performance function  $y$  and failure criteria for the reliability is defined as  $P_F := P(y < 1.6 \times 10^5)$ . Contours of stochastic topology sensitivities for compliance are plotted in Fig. 6. The contours for sensitivities of the three moments follow similar patterns but different value ranges as expected since the sensitivity is eventually related to the stress field. The contour for the sensitivity of failure probability is also similar due to the same reason although distinct colors manifest the value difference. Only 23 FEAs are needed to evaluate the first three moments, probability of failure, and their sensitivities for this 11-dimensional example, illustrating the effectiveness of the proposed method for high-dimensional engineering problems.

## 7. Conclusions

A new framework for stochastic topology sensitivity analysis was developed for solving RTO and RBTO problems commonly encountered in engineering. The framework is grounded on the polynomial dimensional decomposition and the concept of topology derivative. Comparing with previous developments, the new method is capable of providing accurate evaluations of stochastic topology sensitivity owing to the dovetailed topology derivative concept. Furthermore, the new method can efficiently tackle high-dimensional stochastic response functions and their topology sensitivities as a result of the hierarchical structure of PDD which decomposes a high-dimensional function in terms of lower-variate component functions. With these two intrinsic advantages, the new method endows the first three moments and their topology sensitivities with analytical expressions. And it also provides embedded MCS for reliability



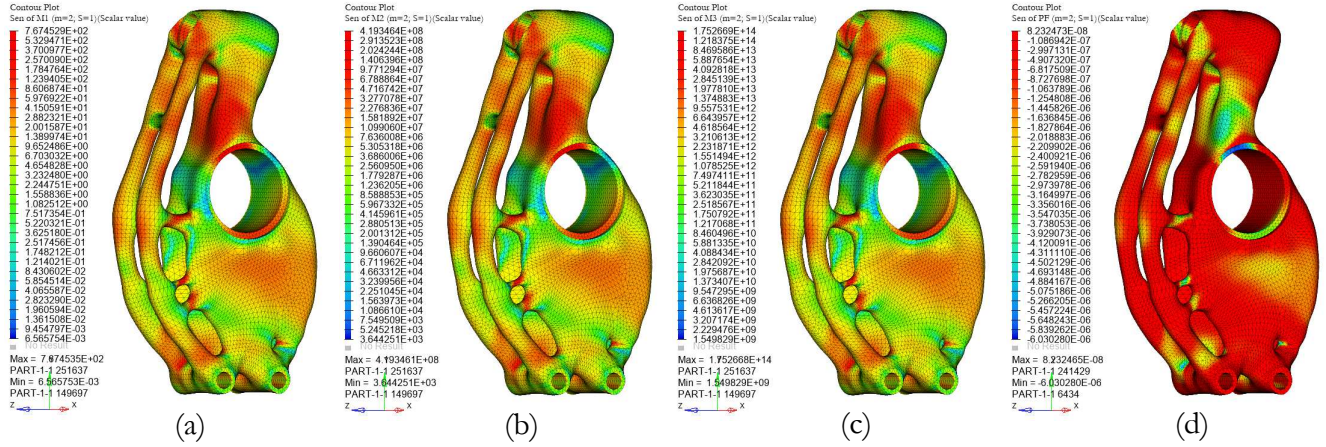


Figure 6: Stochastic topology sensitivity of compliance: (a)-(c) topology sensitivity of 1st moment, 2nd moments, and 3rd moments; (d) topology sensitivity of failure probability

analysis and finite difference formulations for topology sensitivity of reliability. In the finite difference formulations, the definition of topology derivative is utilized as a callback to evaluate the perturbed performance function requiring no additional function evaluations and thus results in a self-consistent framework. It is noteworthy that the evaluation of moments, reliability, and their topology sensitivity is acquired from a single stochastic analysis. In addition, the adjoint method inherited from deterministic topology sensitivity analysis, together with PDD, grant the proposed framework a significantly high efficiency for solving high-dimensional engineering problems especially when FEA is involved.

Two new benchmark examples were developed to address the issue of lacking analytical solutions of stochastic topology sensitivity for verification. The first example provides not only the analytical expression for the first three moments of compliance and their topology sensitivities but also the analytical expression for the failure probability and its topology sensitivity. Aided by this example, the accuracy and efficiency of the proposed method are examined and demonstrated. The second example, accommodating 53 random variables via applying an intricate pressure, supplies analytical solutions for compliance of both the original domain and the perforated domain. These analytical compliances generate exact solutions for the moments and their sensitivities, and also offer a precise evaluation of failure probability via crude Monte Carlo simulation as well as an accurate assessment for its topology sensitivity by virtue of finite difference method. The effectiveness of the proposed method is thus verified and the advantages of the dovetailed decomposition are illustrated by this 53-dimension example. It also demonstrates that topology sensitivities of moments by the proposed method possess higher accuracies than moments themselves when the function structure of deterministic topology derivative is simpler than the response itself. A similar advantage is also observed in the topology sensitivity of failure probability in this example. The proposed method is finally applied to a three-dimension bracket with 11 random variables, by which the application to complex engineering problems is examined.

In summary, the introduction of the topology derivative concept enables a rigorous description of stochastic topology sensitivity and permits the development of new benchmark examples for this research field. The grounded polynomial dimensional decomposition empowers its high efficiency to solve stochastic topology sensitivity for high-dimensional complex engineering problems. In addition, when the deterministic topology derivative of response takes a simpler form than the response itself, the proposed method often supplies better accuracies on stochastic topology sensitivities than on the stochastic analysis.

## Acknowledgments

The authors acknowledge financial support from the U.S. National Science Foundation under Grant No. CMMI-1635167 and the startup funding of Georgia Southern University. Also to commemorate Niels Henrik Abel.

## Appendix A. The solutions for the external problem

The solution of Eq. (16) were well studied by mathematicians in early research [72, 66]. However, topological derivatives require only the solution on the boundary  $\partial\omega_\rho$ , which can be obtained in an easier approach comparing to those in literature [72, 66]. In this appendix, an approach based on Eshelby tensor [73] and solutions for plane stress, plane strain, and three-dimensional cases are compiled for easy accessibility of researchers in mechanics and engineering field. When the elastic medium in Eshelby phase-transition strain problem is isotropic and the inclusion domain  $\Omega$  is a sphere, the Eshelby tensor is isotropic

$$\mathbb{S} = (\alpha - \beta) \frac{1}{3} \delta\delta + \beta \mathbb{I} \quad (\text{A.1})$$

where

$$\alpha = \frac{3K}{3K + 4G}, \quad \beta = \frac{6(K + 2G)}{5(3K + 4G)},$$

and  $G$  and  $K$  are shear modulus and bulk modulus, respectively. The real strain on the boundary of the inclusion reads

$$\hat{\epsilon} = (\mathbb{S}^{-1} - \mathbb{I})^{-1} \mathbb{C}^{-1} : \hat{\sigma} \quad (\text{A.2})$$

where  $\hat{\sigma}$  is the stress on the surface of the inclusion. To utilize it for the solution on  $\partial\omega_\rho$  of Eq. (16), let

$$\hat{\sigma} = \sigma(\xi_0) \quad (\text{A.3})$$

where  $\sigma(\xi_0)$  is the stress at  $\xi_0$  in Eq. (14). Therefore the strain solution for Eq. (16)

$$\hat{\epsilon} = \left( \frac{a-b}{3} \delta\delta + b\mathbb{I} \right) : \sigma(\xi_0) \quad (\text{A.4})$$

where  $a = \frac{1}{4G} = \frac{1+\nu}{2E}$ ,  $b = \frac{3(K+2G)}{G(9K+8G)} = \frac{2(4-5\nu^2-\nu)}{E(7-5\nu)}$ . The corresponding displacement solution on  $\partial\omega_\rho$  reads

$$\begin{aligned} \hat{u} &= \left( \frac{a-b}{3} \delta\delta + b\mathbb{I} \right) : \sigma(\xi_0) \cdot n\rho \\ &= \rho \left( \frac{a-b}{3} \text{tr}(\sigma(\xi_0)) n + bn \cdot \sigma(\xi_0) \right) \end{aligned} \quad (\text{A.5})$$

For plane strain cases, the Eshelby tensor becomes

$$\mathbb{S} = (\alpha - \beta) \frac{1}{2} \delta\delta + \beta \mathbb{I} \quad (\text{A.6})$$

with  $\alpha = \frac{1}{2(1-\nu)}$ ,  $\beta = \frac{3-4\nu}{4(1-\nu)}$ , and the displacement solution on  $\partial\omega_\rho$  becomes

$$\begin{aligned} \hat{u} &= \frac{(1+\nu)}{E} [(2\nu-1) \delta\delta + (3-4\nu) \mathbb{I}] : \sigma(\xi_0) \cdot n\rho \\ &= \rho \frac{(1+\nu)}{E} [(2\nu-1) \text{tr}(\sigma(\xi_0)) n + (3-4\nu) n \cdot \sigma(\xi_0)]. \end{aligned} \quad (\text{A.7})$$

For plane stress cases, simply changing the elastic constant, we have

$$\hat{u} = \rho \left[ \frac{\nu-1}{E} \text{tr}(\sigma(\xi_0)) n + \frac{3-\nu}{E} n \cdot \sigma(\xi_0) \right] \quad (\text{A.8})$$



## References

- [1] Y. Sui, D. Yang, A new method for structural topological optimization based on the concept of independent continuous variables and smooth model, *Acta Mechanica Sinica* 14 (2) (1998) 179–185. 1
- [2] M. Wang, X. Wang, D. Guo, A level set method for structural topology optimization, *Computer Methods in Applied Mechanics and Engineering* 192 (1) (2003) 227–246. 1
- [3] M. Wang, X. Wang, Color level sets: a multi-phase method for structural topology optimization with multiple materials, *Computer Methods in Applied Mechanics and Engineering* 193 (6) (2004) 469–496. 1
- [4] P. Liu, Y. Luo, Z. Kang, Multi-material topology optimization considering interface behavior via xfm and level set method, *Computer Methods in Applied Mechanics and Engineering* 308 (2016) 113–133. 1
- [5] S. Chen, W. Chen, S. Lee, Level set based robust shape and topology optimization under random field uncertainties, *Structural and Multidisciplinary Optimization* 41 (4) (2010) 507–524. 1
- [6] S. Chen, W. Chen, A new level-set based approach to shape and topology optimization under geometric uncertainty, *Structural and Multidisciplinary Optimization* 44 (1) (2011) 1–18. 1
- [7] A. Asadpoure, M. Tootkaboni, J. K. Guest, Robust topology optimization of structures with uncertainties in stiffness—application to truss structures, *Computers & Structures* 89 (11-12) (2011) 1131–1141. 1
- [8] X. Guo, W. Zhang, L. Zhang, Robust structural topology optimization considering boundary uncertainties, *Computer Methods in Applied Mechanics and Engineering* 253 (2013) 356–368. 1
- [9] X. Guo, X. Zhao, W. Zhang, J. Yan, G. Sun, Multi-scale robust design and optimization considering load uncertainties, *Computer Methods in Applied Mechanics and Engineering* 283 (2015) 994–1009. 1
- [10] X. Zhang, Z. Kang, W. Zhang, Robust topology optimization for dynamic compliance minimization under uncertain harmonic excitations with inhomogeneous eigenvalue analysis, *Structural and Multidisciplinary Optimization* 54 (6) (2016) 1469–1484. 1
- [11] L. Jiang, S. Chen, Parametric structural shape & topology optimization with a variational distance-regularized level set method, *Computer Methods in Applied Mechanics and Engineering* 321 (2017) 316–336. 1
- [12] B. Huang, X. Du, Analytical robustness assessment for robust design, *Structural and Multidisciplinary Optimization* 34 (2) (2007) 123–137. 1
- [13] S. Lee, W. Chen, B. Kwak, Robust design with arbitrary distributions using gauss-type quadrature formula, *Structural and Multidisciplinary Optimization* 39 (3) (2009) 227–243. 1
- [14] F. Yamazaki, M. Shinozuka, G. Dasgupta, Neumann expansion for stochastic finite element analysis, *Journal of Engineering Mechanics* 114 (8) (1988) 1335–1354. 1, 2
- [15] N. Kuschel, R. Rackwitz, Two basic problems in reliability-based structural optimization, *Mathematical Methods of Operations Research* 46 (3) (1997) 309–333. 1
- [16] J. Tu, K. K. Choi, Y. H. Park, A new study on reliability-based design optimization, *Journal of Mechanical Design, Transactions of the ASME* 121 (4) (1999) 557–564. 1, 2
- [17] X. P. Du, W. Chen, Sequential optimization and reliability assessment method for efficient probabilistic design, *Journal of Mechanical Design* 126 (2) (2004) 225–233. 1
- [18] A. Chiralaksanakul, S. Mahadevan, First-order approximation methods in reliability-based design optimization, *Journal of Mechanical Design* 127 (5) (2005) 851–857. 1
- [19] H. Agarwal, J. E. Renaud, New decoupled framework for reliability-based design optimization, *AIAA journal* 44 (7) (2006) 1524–1531. 1
- [20] J. H. Liang, Z. P. Mourelatos, E. Nikolaidis, A single-loop approach for system reliability-based design optimization, *Journal of Mechanical Design* 129 (12) (2007) 1215–1224. 1
- [21] H. Wang, N. H. Kim, Robust design using stochastic response surface and sensitivities (2006). 1
- [22] M. Grigoriu, Statistically equivalent solutions of stochastic mechanics problems, *Journal of Engineering Mechanics* 117 (8) (1991) 1906–1918. 1, 2
- [23] H. Xu, S. Rahman, A generalized dimension-reduction method for multidimensional integration in stochastic mechanics, *International Journal for Numerical Methods in Engineering* 61 (12) (2004) 1992–2019. 1, 2, 5
- [24] H. Xu, S. Rahman, Decomposition methods for structural reliability analysis, *Probabilistic Engineering Mechanics* 20 (3) (2005) 239–250. doi:10.1016/j.probenmech.2005.05.005. URL <http://www.sciencedirect.com/science/article/pii/S026689200500010X> 1, 2, 5
- [25] M. Grigoriu, *Stochastic calculus: applications in science and engineering*, Springer, 2002. 1, 2
- [26] S. Amstutz, A. Novotny, E. de Souza Neto, Topological derivative-based topology optimization of structures subject to drucker–prager stress constraints, *Computer Methods in Applied Mechanics and Engineering* 233 (2012) 123–136. 1
- [27] A. A. Novotny, R. A. Feijóo, E. Taroco, C. Padra, Topological sensitivity analysis, *Computer methods in applied mechanics and engineering* 192 (7-8) (2003) 803–829. 1
- [28] G. Allaire, F. De Gournay, F. Jouve, A.-M. Toader, Structural optimization using topological and shape sensitivity via a level set method, *Control and cybernetics* 34 (1) (2005) 59. 1
- [29] W. Zhang, Z. Kang, Robust shape and topology optimization considering geometric uncertainties with stochastic level set perturbation, *International Journal for Numerical Methods in Engineering* 110 (1) (2017) 31–56. 1
- [30] Z. Kang, P. Liu, Reliability-based topology optimization against geometric imperfections with random threshold model, *International Journal for Numerical Methods in Engineering* 115 (1) (2018) 99–116. 1
- [31] X. P. Du, W. Chen, Towards a better understanding of modeling feasibility robustness in engineering design, *Journal of Mechanical Design* 122 (4) (2000) 385–394. 2
- [32] I. Enevoldsen, J. D. Sørensen, Reliability-based optimization in structural engineering, *Structural safety* 15 (3) (1994) 169–196. 2
- [33] E. Rosenblueth, Two-point estimates in probabilities, *Applied Mathematical Modelling* 5 (5) (1981) 329–335. 2
- [34] H. P. Hong, An efficient point estimate method for probabilistic analysis, *Reliability Engineering & System Safety* 59 (3) (1998) 261–267. 2

- [35] M. Kleiber, T. D. Hien, *The stochastic finite element method*, Wiley, 1992. 2
- [36] S. Rahman, B. N. Rao, A perturbation method for stochastic meshless analysis in elastostatics, *International Journal for Numerical Methods in Engineering* 50 (8) (2001) 1969–1991. 2
- [37] D. H. Evans, An application of numerical integration techniques to statistical tolerancing, *Technometrics* 9 (3) (1967) 441–456. 2
- [38] C. A. Cornell, A probability-based structural code\*, in: *ACI Journal Proceedings*, Vol. 66, ACI, 1969, pp. 974–985. 2
- [39] H. O. Madsen, S. Krenk, N. C. Lind, *Methods of structural safety*, Prentice-Hall, Inc., 1986. 2
- [40] A. M. Hasofer, N. C. Lind, Exact and invariant second-moment code format, *Journal of the Engineering Mechanics Division* 100 (1) (1974) 111–121. 2
- [41] B. Fiessler, R. Rackwitz, H. J. Neumann, Quadratic limit states in structural reliability, *Journal of the Engineering Mechanics Division* 105 (4) (1979) 661–676. 2
- [42] M. Hohenbichler, R. Rackwitz, Non-normal dependent vectors in structural safety, *Journal of the Engineering Mechanics Division* 107 (6) (1981) 1227–1238. 2
- [43] K. Breitung, Asymptotic approximations for multinormal integrals, *Journal of Engineering Mechanics* 110 (3) (1984) 357–366. 2
- [44] A. Der Kiureghian, H. Z. Lin, S. J. Hwang, Second-order reliability approximations, *Journal of Engineering Mechanics* 113 (8) (1987) 1208–1225. 2
- [45] Y. T. Wu, H. R. Millwater, T. A. Cruse, Advanced probabilistic structural analysis method for implicit performance functions, *AIAA Journal* 28 (9) (1990) 1663–1669. 2
- [46] Y. T. Wu, P. H. Wirsching, New algorithm for structural reliability estimation, *Journal of Engineering Mechanics* 113 (9) (1987) 1319–1336. 2
- [47] P. L. Liu, A. Der Kiureghian, Optimization algorithms for structural reliability, *Structural Safety* 9 (3) (1991) 161–177. 2
- [48] S. Rahman, A polynomial dimensional decomposition for stochastic computing, *International Journal for Numerical Methods in Engineering* 76 (13) (2008) 2091–2116. 3.1, 3.1, 3.1
- [49] S. Rahman, Extended polynomial dimensional decomposition for arbitrary probability distributions, *Journal of Engineering Mechanics-ASCE* 135 (12) (2009) 1439–1451. 3.1, 3.1, 3.1
- [50] S. Rahman, Statistical moments of polynomial dimensional decomposition, *Journal of Engineering Mechanics* 136 (7) (2010) 923–927. 3.2, 3.2
- [51] X. Ren, S. Rahman, Robust design optimization by polynomial dimensional decomposition, *Structural and Multidisciplinary Optimization* 48 (1) (2013) 127–148. 3.3, 4.2
- [52] S. Rahman, X. Ren, Novel computational methods for high-dimensional stochastic sensitivity analysis, *International Journal for Numerical Methods in Engineering* 98 (12) (2014) 881–916. 3.3, 4.2
- [53] X. Ren, V. Yadav, S. Rahman, Reliability-based design optimization by adaptive-sparse polynomial dimensional decomposition, *Structural and Multidisciplinary Optimization* (2015) 1–28. 3.3
- [54] J. Sokolowski, A. Zochowski, On the topological derivative in shape optimization, *Siam Journal on Control and Optimization* 37 (4) (1999) 1251–1272. 4
- [55] J. Sokolowski, A. Zochowski, Topological derivatives of shape functionals for elasticity systems, *Mechanics of Structures and Machines* 29 (3) (2001) 331–349. 4
- [56] M. Burger, B. Hackl, W. Ring, Incorporating topological derivatives into level set methods, *Journal of Computational Physics* 194 (1) (2004) 344–362. 4
- [57] S. Amstutz, A. A. Novotny, E. A. D. Neto, Topological derivative-based topology optimization of structures subject to drucker-prager stress constraints, *Computer Methods in Applied Mechanics and Engineering* 233 (2012) 123–136. 4
- [58] D. Bojczuk, Z. Mroz, Topological sensitivity derivative and finite topology modifications: application to optimization of plates in bending, *Structural and Multidisciplinary Optimization* 39 (1) (2009) 1–15. 4
- [59] J. A. Norato, M. P. Bendsoe, R. B. Haber, D. A. Tortorelli, A topological derivative method for topology optimization, *Structural and Multidisciplinary Optimization* 33 (4-5) (2007) 375–386. 4
- [60] G. Allaire, F. de Gournay, F. Jouve, A. M. Toader, Structural optimization using topological and shape sensitivity via a level set method, *Control and Cybernetics* 34 (1) (2005) 59–80. 4
- [61] G. Allaire, F. Jouve, A. M. Toader, Structural optimization using sensitivity analysis and a level-set method, *Journal of Computational Physics* 194 (1) (2004) 363–393. 4
- [62] S. Amstutz, Connections between topological sensitivity analysis and material interpolation schemes in topology optimization, *Structural and Multidisciplinary Optimization* 43 (6) (2011) 755–765. 4
- [63] A. Shumacher, *Topologieoptimierung von bauteilstrukturen unter verwendung von lochpositionierungskriterien*, These de doctorat, Universitat-Gesamthochschule-Siegen, Siegen (1995). 4.1
- [64] J. Sokolowski, A. Zochowski, Topological derivatives for elliptic problems, *Inverse problems* 15 (1) (1999) 123. 4.1
- [65] J. Sokolowski, A. Zochowski, Topological derivative in shape optimization, *Encyclopedia of Optimization* (2009) 3908–3918. 4.1
- [66] S. Garreau, P. Guillaume, M. Masmoudi, The topological asymptotic for pde systems: the elasticity case, *SIAM journal on control and optimization* 39 (6) (2001) 1756–1778. 4.1, 4.1, Appendix A, Appendix A
- [67] I. Busbridge, Some integrals involving hermite polynomials, *Journal of the London Mathematical Society* 23 (1948) 135–141. 4.2
- [68] X. Ren, S. Rahman, Robust design optimization by polynomial dimensional decomposition, *Structural and Multidisciplinary Optimization* 48 (1) (2013) 127–148. 4.2
- [69] S. Rahman, H. Xu, A univariate dimension-reduction method for multi-dimensional integration in stochastic mechanics, *Probabilistic Engineering Mechanics* 19 (4) (2004) 393–408. 5
- [70] N. Muskhelishvili, *Some basic problems of the mathematical theory of elasticity*, Noordhoff, Groningen 17404 (1963). 6.2.1
- [71] Grabcad - bracket topology optimization 3, <https://grabcad.com/library/bracket-topology-optimization-3-1>, online; accessed 22-July-2019 (2019). 6.3
- [72] R. W. Little, *Elasticity* prentice-hall, Englewood Cliffs, NJ (1973) 88–94. Appendix A, Appendix A

[73] J. Eshelby, The elastic energy-momentum tensor, *Journal of elasticity* 5 (3-4) (1975) 321–335. Appendix A